Bubble Screen Shielding of Water Pressure Waves Emitted by a Harmonically Pulsating Vessel

K.J. O'Brien and G.A. Moses

July 1982

UWFDM-476

FUSION TECHNOLOGY INSTITUTE

UNIVERSITY OF WISCONSIN

MADISON WISCONSIN

Bubble Screen Shielding of Water Pressure Waves Emitted by a Harmonically Pulsating Vessel

K.J. O'Brien and G.A. Moses

Fusion Technology Institute
University of Wisconsin
1500 Engineering Drive
Madison, WI 53706

http://fti.neep.wisc.edu

July 1982

UWFDM-476

Table of Contents

ABSTRACT

It has been proposed to investigate[1] the possibility of surrounding the target chamber of the Light Ion Beam Target Development Facility with a water shield. Such a shield would effectively isolate the chamber from the environment while providing a medium in which to absorb energy imparted to the target chamber following impact of the fireball.

If the water surrounding the chamber provides a damping mechanism for the wall vibrations, it also provides a medium through which a pressure pulse can be transmitted to the outer wall of the shield region. It is desirable to minimize the pressure loading upon this structure.

A preliminary investigation of the effects of a bubble screen upon the propagation of the water pressure wave is presented, along with some possible criteria for the design of a screen. It is found that, while a screen effectively shields the outer wall, reflection back to the target chamber occurs. A screen must be tuned for an optimum balance between reflection, transmission and absorption.

Estimates of the fluid pressure amplitudes are arrived at by modeling the target chamber as a harmonically pulsating vessel and solving for the resultant fluid motions. For purposes of analyzing the screen an incident plane wave with comparable amplitude is employed.

1. INTRODUCTION

In this report we present calculations of the propagation of acoustic waves generated by a pulsating vessel submerged in a large water filled pool. In addition we calculate the reflection, attenuation, and transmission of these acoustic waves by bubble filled regions in the water tank. This is shown schematically in Fig. 1.

This work was motivated by design activities on the Light Ion Beam Fusion Target Development Facility[1] depicted in Fig. 2. In this facility a light ion beam driven target is exploded inside of the vessel shown in the center of Fig. 2. The vessel is filled with approximately 20 torr of gas to support the propagation of the ion beams through preformed plasma channels from diodes to the target. This gas subsequently absorbs the x-ray and ionic debris emanating from the target, creating a micro-fireball that propagates to the wall of the vessel. The wall of the vessel must be designed to withstand the blast pressure and heat flux from the fireball.

Approximately 30% of the fusion energy is released in the form of x-rays and ionic debris. The remainder comes in the form of high energy neutrons. Thus there is the need for substantial amounts of neutron shielding around this reaction vessel to protect operating personnel and to avoid activation of the surrounding pulsed power machine that generates the energy to drive the ion diodes. Since this is meant to be an experimental facility it is also desirable that there be easy access to the vessel and the diodes. In this situation a water shield in the region between the vessel and the water dielectric section of the pulsed power machine is an obvious choice. It can be easily drained to give access to the vessel for maintenance.

Fig. 1

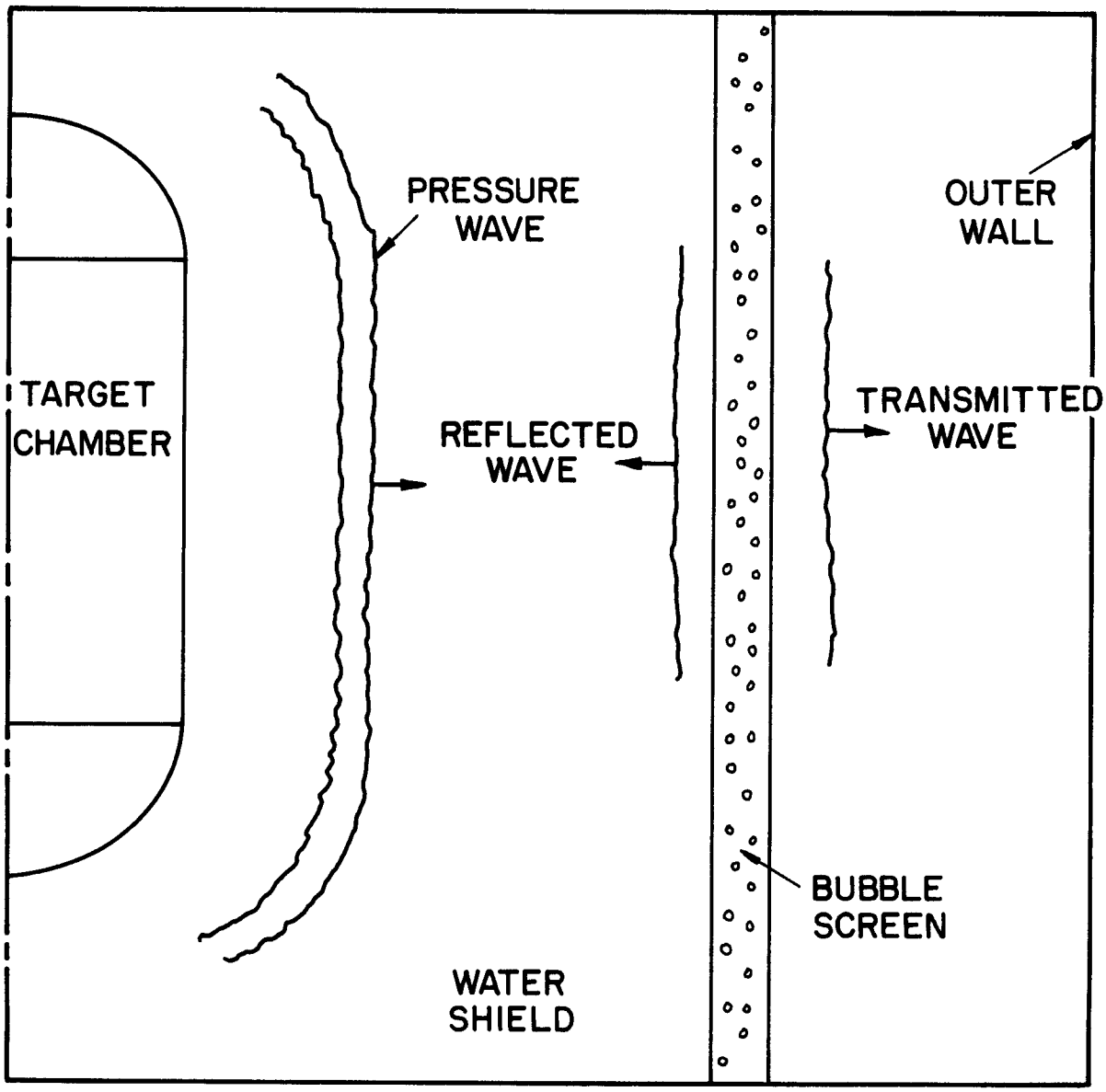
PRESSURE
WAVE
OUTER
WALL
TARGET
CHAMBER
REFLECTED
WAVE
TRANSMITTED
WAVE
BUBBLE
SCREEN
WATER
SHIELD

Fig. 2

Light Ion Beam Target Development Facility

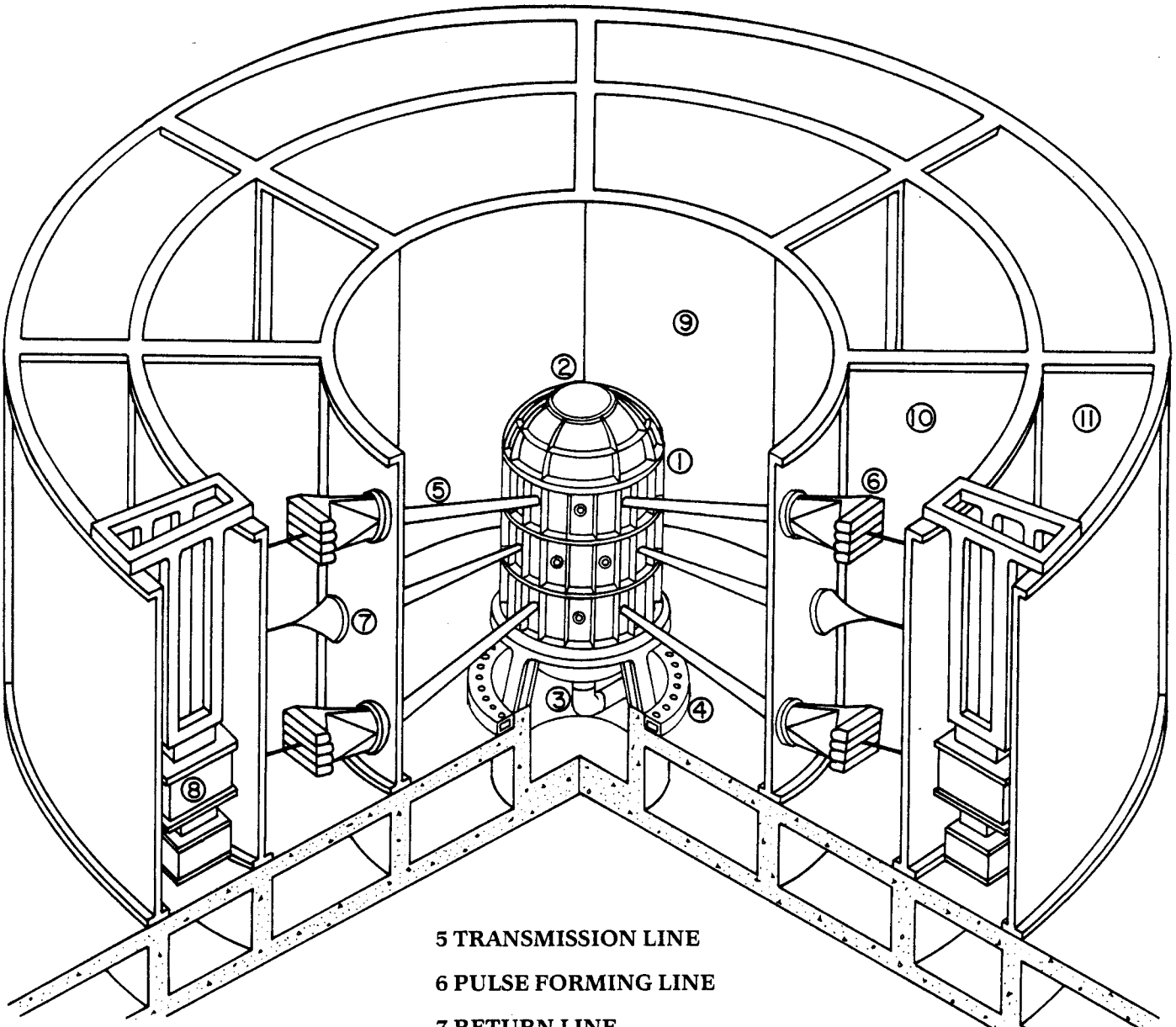

1 TARGET CHAMBER

2 DIAGNOSTIC PORT

3 PURGE LINE

4 AIR BUBBLE PLENUM

5 TRANSMISSION LINE

6 PULSE FORMING LINE

7 RETURN LINE

8 BEAM MARX GENERATOR

9 SHIELDING POOL – WATER

10 PULSE FORMING SECTION – WATER

11 ENERGY STORAGE SECTION – OIL

However, this concept does present some technical difficulties. The shock overpressure on the vessel wall created by the micro-fireball sends the wall into a vibrating motion, thus transmitting the overpressure into the surrounding water shield. This disturbance will propagate through the water to the wall separating the water shield from the water section of the pulsed power machine. It will propagate through this wall, into the water section, and possibly damage the pulse forming lines or other components.

A proposed solution to this problem is the introduction of a bubble "screen" in the water shield that would attenuate the pressure wave. To provide the basis for the analysis of this design we have investigated the propagation of cylindrically and spherically divergent acoustic waves radiated from a pulsating source. We have verified that the linear acoustic theory is applicable to our particular set of conditions. Knowing the structure and amplitude of the waves we analyzed the interaction of these waves when they are incident upon a bubble filled region of finite thickness. We calculate the reflection, attenuation and transmission of waves in general, and for our particular set of circumstances.

1.1 Formulation of the Problem

A conceptual picture of the Light Ion Beam Target Development Facility is shown[1] in Fig. 2. The target explosion within the target chamber generates a blast wave which propagates through the cavity gas, transmitting a pulsed heat flux and shock overpressure to the first wall. Maximum overpressures have been estimated using computer simulations.[2] Figure 3 shows a typical result for a particular choice of design parameters.

The target chamber is supposed to be constructed of plates and stringers, Fig. 4. The frame is modeled as a system of beams in which the curvature and

Figure 3 Heat flux and shock overpressure on a 3 meter radius first wall resulting from a 200 MJ microexplosion in a 70 torr gas of xenon with 0.5% cesium.

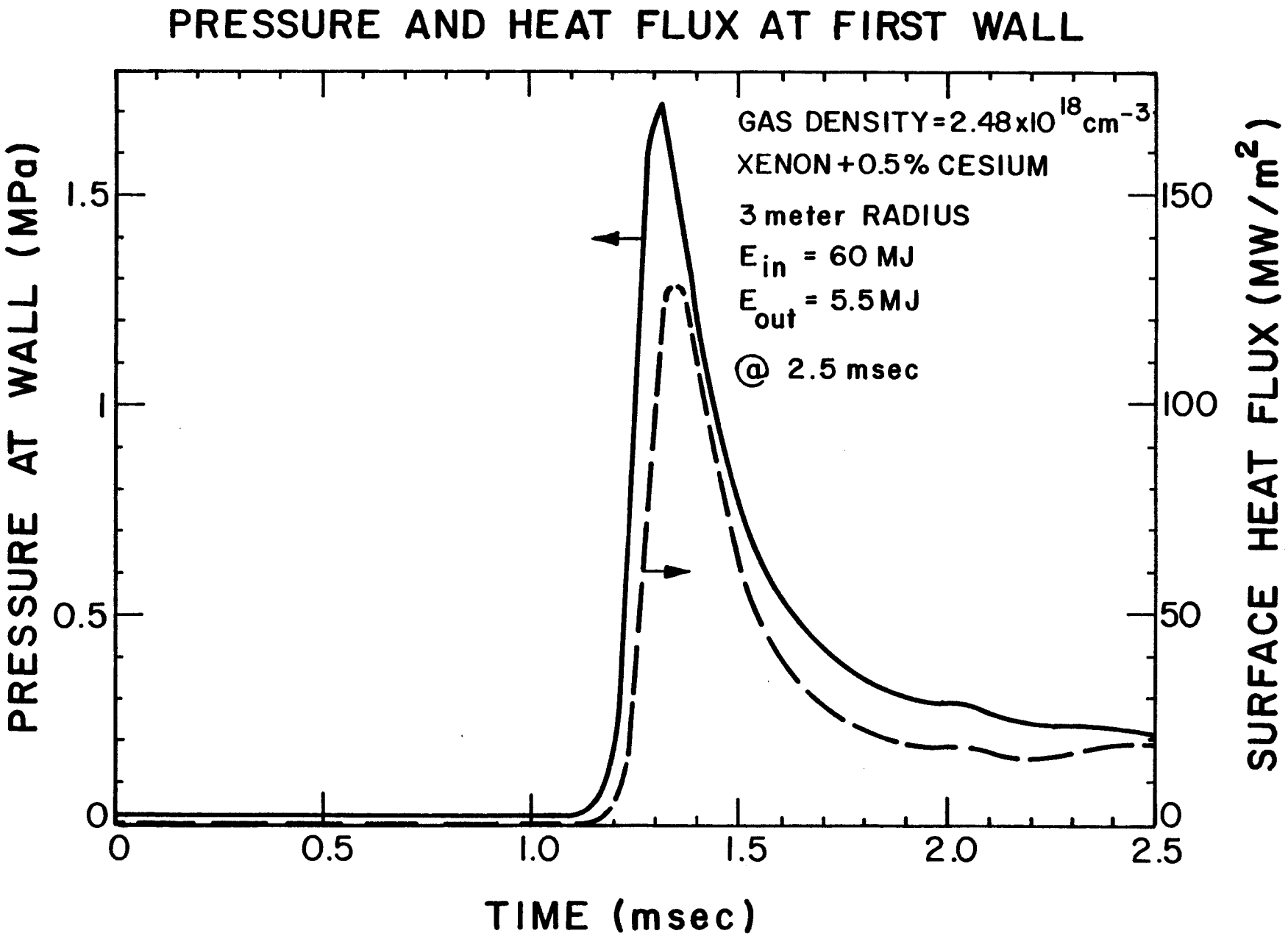

Fig. 4

CONCEPTUAL FIRST WALL
STRUCTURAL SYSTEM

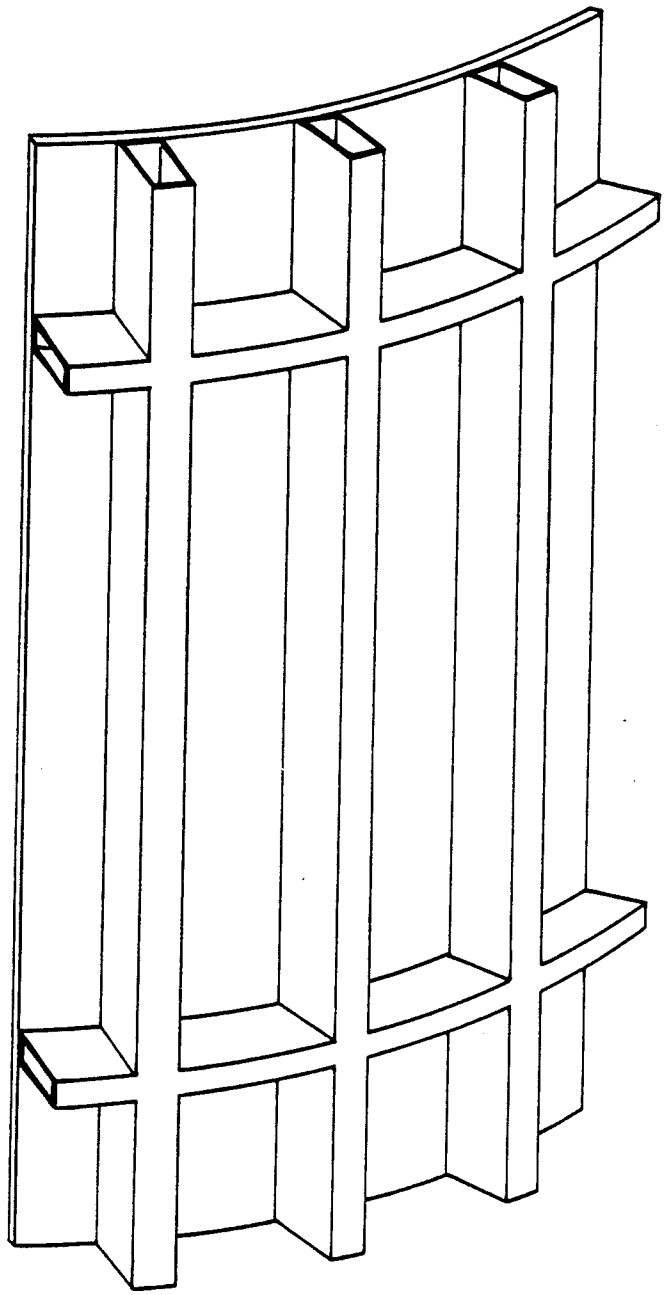

hoop force capacity of the beams is not included, the plates are assumed to transmit the full strength of the overpressure, without resistance from circumferential tensile stresses.[3] Dynamics of first wall response is treated in detail in Refs. (3) and (4).

Detailed modeling of the response of a plate section yields the time behavior of the maximum deflection point. After a short transient time the motion is harmonic and damps exponentially. Damping is dependent upon internal dissipative mechanisms such as strain energy. Previous analysis of the plate motion has included no external damping forces.

For the purposes of this study the structure of the vessel wall will be simplified considerably, with plates and stringers eliminated completely. The target chamber will be modeled as a single component, of uniform composition, comprised of a cylindrical barrel with hemispherical caps. This vessel will pulsate harmonically in the same fashion as the maximum deflection point of a plate. Transient effects will be ignored, the wall begins damped oscillations at time zero with maximum velocity taken (unphysically) at this time. This has no effect upon further analysis except to eliminate the transient wavefront emitted by the vessel during this time.

This model presents a worst case treatment as far as the outer wall is concerned. Due to the complicated rib-plate structure a real wall would not be expected to emit perfect cylindrical or hemispherical waves. In this case it is expected that the overpressures at the outer wall would be diminished; due to the randomizing effect of the vessel wall much of the energy would be emitted nonradially. Further, the deflection amplitude is over-estimated and should be taken as a mean deflection over a plate surface.[5]

Complicated reflection patterns, associated with a free-surface and a zero-velocity surface, will develop in the water shield. These effects are ignored with the assumption of a chamber surrounded by an infinite shield.

A cylindrical bubble screen, concentric with the vessel, is generated by a plenum as shown in Fig. 2. Since the screen is assumed to be located some distance from the chamber it will prove adequate to consider only plane waves incident upon a bubble slab.

1.2 Cavitation at the Water-Wall Interface

Before considering the propagation of acoustic waves in the water we look at the conditions that are necessary to avoid cavitation at the wall-water interface. Cavitation in this region might change the character of the transmitted pressure wave. Water supports very little tension, consequently, for violent wall pulsations, water may break away from the wall, forming local boiling and turbulence. This cavitation results from negative instantaneous pressure at the water-wall interface, thus the concern is with pulsations that create pressure amplitudes greater than the hydrostatic plus atmospheric pressure.

The acoustic intensity of a sound wave (average power transmitted per unit area) is given by

$$I = \frac{p_{peak}^2}{2\rho c}$$

where c is the sound of speed and ρ the density of the medium through which the wave is propagating. This is also the power per unit area emitted by the wall, hence cavitation will occur if

$$\sqrt{2\ I\rho c} > P_o$$

where P_o is the ambient pressure at the water-wall interface.

The sound speed in a one-component, two-phase mixture is dramatically decreased with respect to the sound speed in either the pure vapor or the pure fluid p e. An asymptotic result, valid for void fractions X << 1 is[6]

$$c = q\mu PV_1/RT \sqrt{c_{P_1} T}$$

where: R = gas constant

V_1 = liquid specific volume

μ = molecular weight

P = pressure

T = absolute temperature

c_{P_1} = liquid specific heat at constant pressure.

Formation of voids at the water-wall interface will decrease the sound speed in a thin sheath surrounding the vessel wall. Voids will form on the compression cycle and condense out on the expansion cycle of the wall. Whereas shocks are not expected to be launched into pure water in the case of the TDF they could be launched into this two-phase boundary region if the sound speed were less than the wall speed at some point of the expansion cycle. Even when most of the voids have been condensed out, the sound speed is greatly decreased.

Finally, the fact that the water at the water-wall interface will be exposed to a neutron flux could increase the likelihood of void formation.[7]

A major assumption will be that void formation will not appreciably change any of the important characteristics of the wave ultimately impinging on the outer wall.

2. ANALYSIS OF WATER PRESSURE WAVES EMMITED BY A PULSATING VESSEL

In this section a nonlinear treatment of the fluid dynamics, allowing the possibility of shocks, is presented. The equations are then specialized to the linear accoustic case for the remainder of the analysis. The basic hydrodynamic equations governing wave motion in a fluid are

$$\frac{\partial}{\partial t}\rho(\vec{r},t) + \vec{\nabla}\cdot\rho(\vec{r},t)\vec{V}(\vec{r},t) = 0 \tag{1}$$

$$\frac{d}{dt}\rho(\vec{r},t)\vec{V}(\vec{r},t) = -\vec{\nabla}P(\vec{r},t) - \vec{\nabla}\cdot\overleftrightarrow{\tau}(\vec{r},t) + \rho(\vec{r},t)\vec{g} \tag{2}$$

$$P(\vec{r},t) = P\left(\rho(\vec{r},t), s(\vec{r},t)\right) \tag{3}$$

$$\frac{d}{dt}s(\vec{r},t) = 0 \ . \tag{4}$$

Equation (4), which is the specific entropy transport equation is a consequence of assuming reversible adiabatic changes behind the wave front. This condition is achieved if the influence of heat conduction and diffusion can be neglected in the time interval during which an element of fluid is traversed by the wave. In reality all elements of the wave are not on the same adiabat. For cylindrical or spherical waves the wave front is of changing intensity so that the entropy increment of a fluid element depends upon the time at which it passed through the wave front.[8]

There are six equations to determine:

$$\rho(\vec{r},t) \qquad s(\vec{r},t) \qquad \vec{V}(\vec{r},t)$$

$$P(\vec{r},t)$$

Neglecting the stresses due to viscosity and assuming only radial dependence the basic equations reduce to:

$$\rho(r,t)\frac{\partial V}{\partial t}(r,t) + \rho(r,t)V(r,t)\frac{\partial V}{\partial r}(r,t) = -\frac{\partial}{\partial r}P(r,t) \tag{5}$$

$$\frac{\partial}{\partial t}\rho(r,t) + \frac{1}{r^k}\frac{\partial}{\partial r}\left(\rho(r,t)V(r,t)r^k\right) = 0 \ . \tag{6}$$

Following Ref. (8), the Tait equation of state along an adiabat is employed

$$\frac{\rho_o}{\rho}\left(\frac{\partial\rho}{\partial P}\right)_T = \frac{1}{n\left(\frac{\rho_o c_o^2}{n} + P\right)} \tag{7}$$

with n = 7. The entropy equation (4) is then no longer needed. With the introduction of a velocity potential there results:

$$V(r,t) = \frac{\partial}{\partial r}\phi(r,t) \tag{8}$$

$$\nabla^2\phi - \frac{1}{c^2}\frac{\partial^2\phi}{\partial t^2} = \frac{1}{c^2}\left(\frac{\vec{V}}{2}\cdot\vec{\nabla}\vec{V}^2 - \frac{d}{dt}V^2\right) \ . \tag{9}$$

The nonlinear wave equation (6) specializes to

$$\frac{\partial^2}{\partial r^2}(r\phi) - \frac{1}{c^2}\frac{\partial^2}{\partial t^2}(r\phi) = \frac{r}{c^2}\left(\frac{V}{2}\frac{\partial V^2}{\partial r} - \frac{dV^2}{dt}\right) \tag{10}$$

for the spherical wave, and to

$$\frac{1}{r}\frac{\partial}{\partial r}\frac{1}{r}\frac{\partial \phi}{\partial r} - \frac{1}{c^2}\frac{\partial^2 \phi}{\partial t^2} = \frac{1}{c^2}\left(\frac{V}{2}\frac{\partial V^2}{\partial r} - \frac{dV^2}{dt}\right) \tag{11}$$

for the cylindrical wave. Boundary conditions are:

$$\frac{\partial \phi}{\partial r}(R_{wall},t) = V_{wall}(t)$$

$$\phi(r,\infty) = 0$$

$$\phi(\infty,t) < \infty$$

$$\phi(r,0) = 0 \qquad r > R_{wall} \ .$$

Determination of the pressure proceeds from the continuity equation

$$\left(\frac{\partial}{\partial t} + V\frac{\partial}{\partial r} + \frac{\partial V}{\partial r} + \frac{kV}{r}\right)\rho(r,t) = 0 \ . \tag{12}$$

With the definition

$$\xi(r,t) = -\left(\frac{\partial V}{\partial r} + \frac{kV}{r}\right) \tag{13}$$

the continuity equation is written as

$$\left(\frac{\partial}{\partial t} + V\frac{\partial}{\partial r}\right)\rho(r,t) = \xi(r,t)\rho(r,t) \tag{14}$$

from which we get

$$\frac{d\rho}{dr} = \frac{\xi}{V} \qquad \frac{d\rho}{dt} = \xi \qquad \frac{dr}{dt} = V \tag{15}$$

along a characteristic. Finally, the equation of state closes the system

$$P(r,t) = \frac{\rho_o c_o^2}{n} \left[\frac{\rho^2(r,t)}{\rho_o^2} - 1\right] . \tag{16}$$

Given the wall velocity $V(R_w,t)$ this system of equations can be solved for the pressure wave in the fluid. This method will not be employed fully but will be reduced to the acoustic limit by showing that the nonlinear terms are of little consequence for the wall motions under consideration.

2.1 Spherical Wave Case

2.1.1 Spherical Waves

If we neglect the nonlinear terms in Eqs. (8) and (9), they become

$$\nabla^2(r\phi) - \frac{1}{c^2} \frac{\partial^2}{\partial t^2} (r\phi) = 0 \tag{17}$$

$$V = \frac{\partial \phi}{\partial r}$$

$$\rho_o \frac{\partial V}{\partial t} = - \frac{\partial P}{\partial r} .$$

2.1.2 Undamped Case

The solution of these equations for the velocity, assuming undamped harmonic wall pulsations $V_w(t) = V_w \cos \omega t$, $t \geq 0$ is

$$V(r,t) = \frac{V_w R_w^2}{c^2 + R_w^2\omega^2} \frac{1}{r^2} \left[(c^2 + R_w r\omega)\cos\ \omega\left(t - \frac{r - R_w}{c}\right)\right. \tag{18}$$

$$\left. - c\omega(r - R_w)\sin\ \omega\left(t - \frac{r - R_w}{c}\right)\right] + \frac{V_w c^2 R_w}{c^2 + R_w^2\omega^2} \frac{r - R_w}{r} e^{-\frac{c}{R_w}\left(t - \frac{r-R_w}{c}\right)}$$

valid for $t < (r - R_w)/c$.[17]

2.1.3 Evaluation of Nonlinear Terms

The previous linear result can be used to estimate the nonlinear effects. We substitute this expression for velocity into the nonlinear term

$$\frac{1}{c^2}\left(\frac{V}{2}\frac{\partial V^2}{\partial r} - \frac{dV^2}{dt}\right) \tag{19}$$

at the wall, at time zero, and this yields

$$-\frac{1}{c^2} V_w^2 \left(\frac{\partial V}{\partial r}\right)_{wall} = \left(\frac{V_w}{c}\right)^2 \frac{V_w}{R_w} . \tag{20}$$

For the wall pulsations under consideration a typical velocity is not greater than 10 m/s. We find

$$\left(\frac{\partial V}{\partial r} + \frac{2}{r} V - \frac{r}{c^2}\frac{\partial^2 \phi}{\partial t^2}\right)_{wall} = \frac{V_w}{R_w} - \frac{R_w}{c^2}\frac{\partial^2 \phi}{\partial t^2} \tag{21}$$

so that the ratio of nonlinear/linear effects is

$$\left(\frac{V_w}{c}\right)^2 << 1 . \tag{22}$$

2.1.4 Damped Case

When we introduce a damping function $\gamma(t)$ the wall velocity can be represented by

$$V_w(t) = \begin{cases} 0 & t < 0 \\ V_w\gamma(t)\cos \omega t & t \geq 0 \ . \end{cases} \tag{23}$$

In this case we can solve for the fluid velocity using Laplace transforms:

$$\overline{V}(r,s) = V_w \mathrm{Re}[\overline{\gamma}(s - i\omega)] \frac{\frac{c}{r} + s}{\frac{c}{R_w} + s} e^{-s\frac{r-R_w}{c}} \tag{24}$$

where

$$\overline{\gamma}(s - i\omega) = L[\gamma(t)e^{i\omega t}] \ .$$

Exponential damping $\gamma(t) = e^{-\gamma t}$ is assumed so that:

$$\overline{V}(r,s) = V_w \frac{R_w}{r} L^{-1}\left[\frac{s + \gamma}{(s + \gamma)^2} \frac{\frac{c}{r} + s}{\frac{c}{R_w} + s} e^{-s\frac{r-R_w}{c}}\right] . \tag{25}$$

Inverting this expression, the velocity is determined to be

$$V(r,t) = \frac{V_w R_w}{(\frac{c}{R_w} - \gamma)^2 + \omega^2} \frac{1}{r^2} e^{-\gamma(t - \frac{r-R_w}{c})} \{\frac{c}{R_w}(\frac{c}{R_w} - \gamma)(r - R_w)e^{-(\frac{c}{R_w} - \gamma)(t - \frac{r-R_w}{c})}$$

$$+ [c(\frac{c}{R_w} - \gamma) + \omega^2 - \gamma(\frac{c}{R_w} - \gamma)r]\cos \omega(t - \frac{r - R_w}{c}) \tag{26}$$

$$- \omega \frac{c}{R_w}(r - R_w)\sin \omega(t - \frac{r - R_w}{c})\} \ .$$

To determine the important quantity, which is P(r,t), the relation

$$\overline{P}(r,s) = \mathrm{Re}\left[\frac{i\omega - \gamma}{\frac{1}{r} + i\frac{\omega}{c}}\rho\overline{V}(r,s)\right] \tag{27}$$

is employed. The result is

$$P(r,t) = \frac{\rho_o V_w}{(1 - r^2\frac{\omega^2}{c^2})(\omega^2 + (\frac{c}{R_w} - \gamma)^2)}\frac{R_w}{r}\left[(A\cos\omega(t - \frac{r - R_w}{c}) + B\sin\omega(t - \frac{r - R_w}{c}))e^{-\gamma(t - \frac{r-R_w}{c})} + Ce^{-\frac{c}{R_w}(t - \frac{r-R_w}{c})}\right] \tag{28}$$

where

$$A = r^2\omega^2(\frac{\omega^2 + \gamma^2}{c} - \frac{\partial\gamma}{R_w}) + r(\frac{c\gamma^2}{R_w} - \gamma(\gamma^2 + \omega^2)) + (c(\gamma^2 + \omega^2) - \frac{c^2\gamma}{R_w})$$

$$B = r^2(\frac{\omega\gamma}{c}(\gamma^2 + \omega^2) + \frac{\omega}{R_w}(\omega^2 - \gamma^2)) + r(-\frac{\omega c\gamma}{R_w}) + \frac{\omega c^2}{R_w} \tag{29}$$

$$C = r^2(\frac{\omega^2 c}{R_w^2}) + r(c\frac{\gamma^2 + \omega^2}{R_w} - \frac{c^2\gamma}{R_w} - \frac{\omega^2 c}{R_w}) + (\frac{c^2\gamma}{R_w} - (\gamma^2 + \omega^2)c) .$$

This function is depicted in Fig. 5. All physical parameters and design parameters are as in Table 1. The plot depicts the wave fronts for times 0.1 to 0.7 ms. The wave fronts end abruptly since the motion of the wall is assumed, unphysically, to begin at time zero at maximum velocity on the expansion cycle. The detailed structure of the wave front beyond the abrupt termination depends upon the initial movements of the wall during the transient period, as discussed earlier. Figure 6 depicts the same wave for times 4.1 to 4.7 ms as it impinges upon the outer wall. The pressure amplitude at the outer wall at

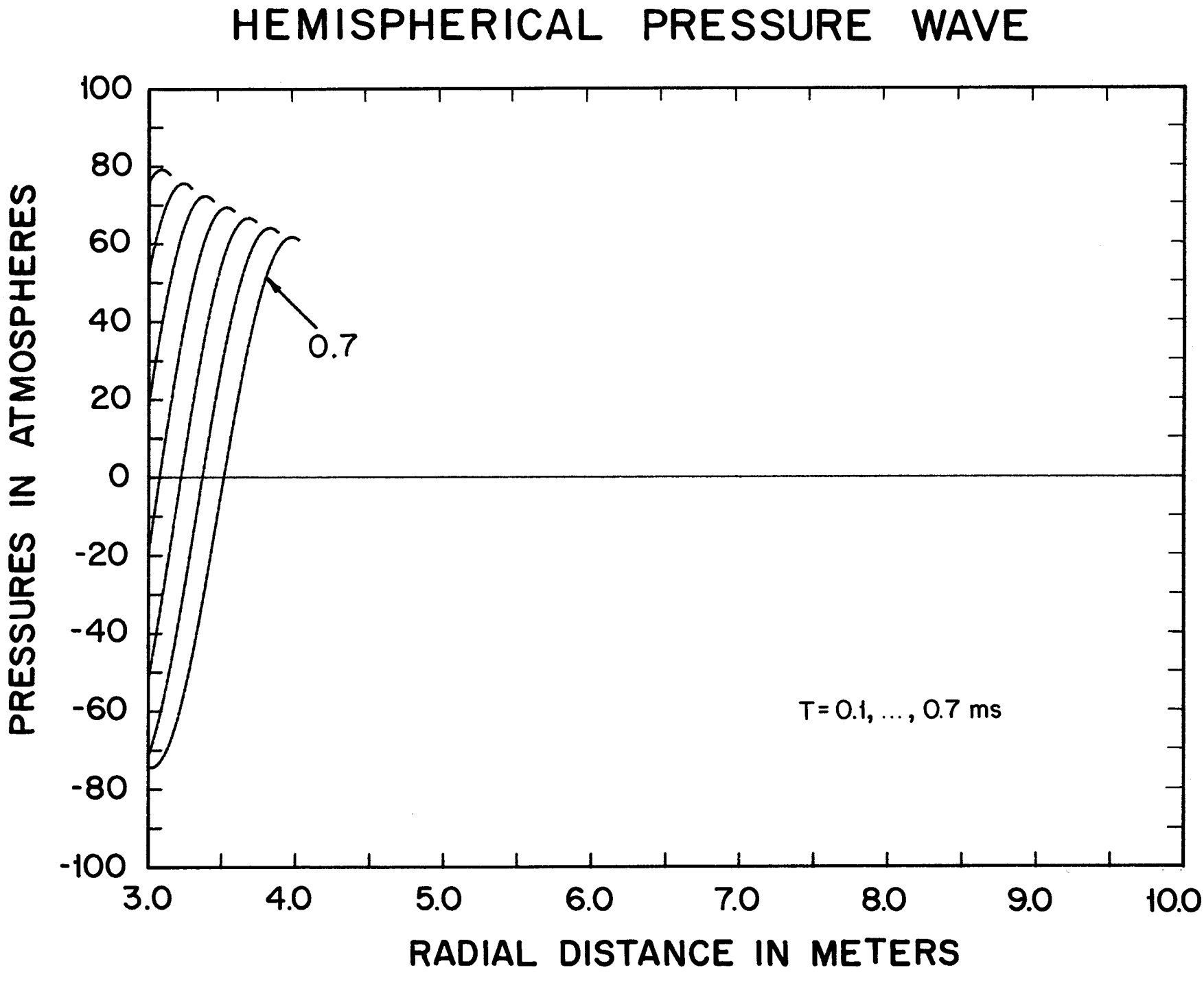
HEMISPHERICAL PRESSURE WAVE
PRESSURES IN ATMOSPHERES
100
80
60
40
20
0
-20
-40
-60
-80
-100
0.7
T= 0.1, ..., 0.7 ms
3.0
4.0
5.0
6.0
7.0
8.0
9.0
10.0
RADIAL DISTANCE IN METERS

Figure 5

Table 1. Specific Parameters for Acoustic Wave and Bubble Screen Calculations

Target Chamber Parameters

R_w = 3 m barrel and hemisphere radius

H_w = 6 m barrel height

ω = 4838 sec^{-1} vibration angular frequency

V_w = 5.7 m/s maximum wall velocity

E = 60 MJ blast wave hydrodynamic energy per shot

γ = 0.118 ms^{-1} damping constant

Fluid Physical Data

ρ_o = 10^3 kg/m^3 water density

c = 1470 m/s sound speed

κ_w = $4.76*10^{-10}$ m^2/nt compressibility

Bubble Physical Data

R_o = 4 mm resonant bubble radius

R_b = 2 mm bubble radius

δ_o = 0.02 bubble resonant damping constant

σ = 0.07 J/m^2 bubble surface tension

κ_b = $5*10^{-6}$ m^2/nt compressibility

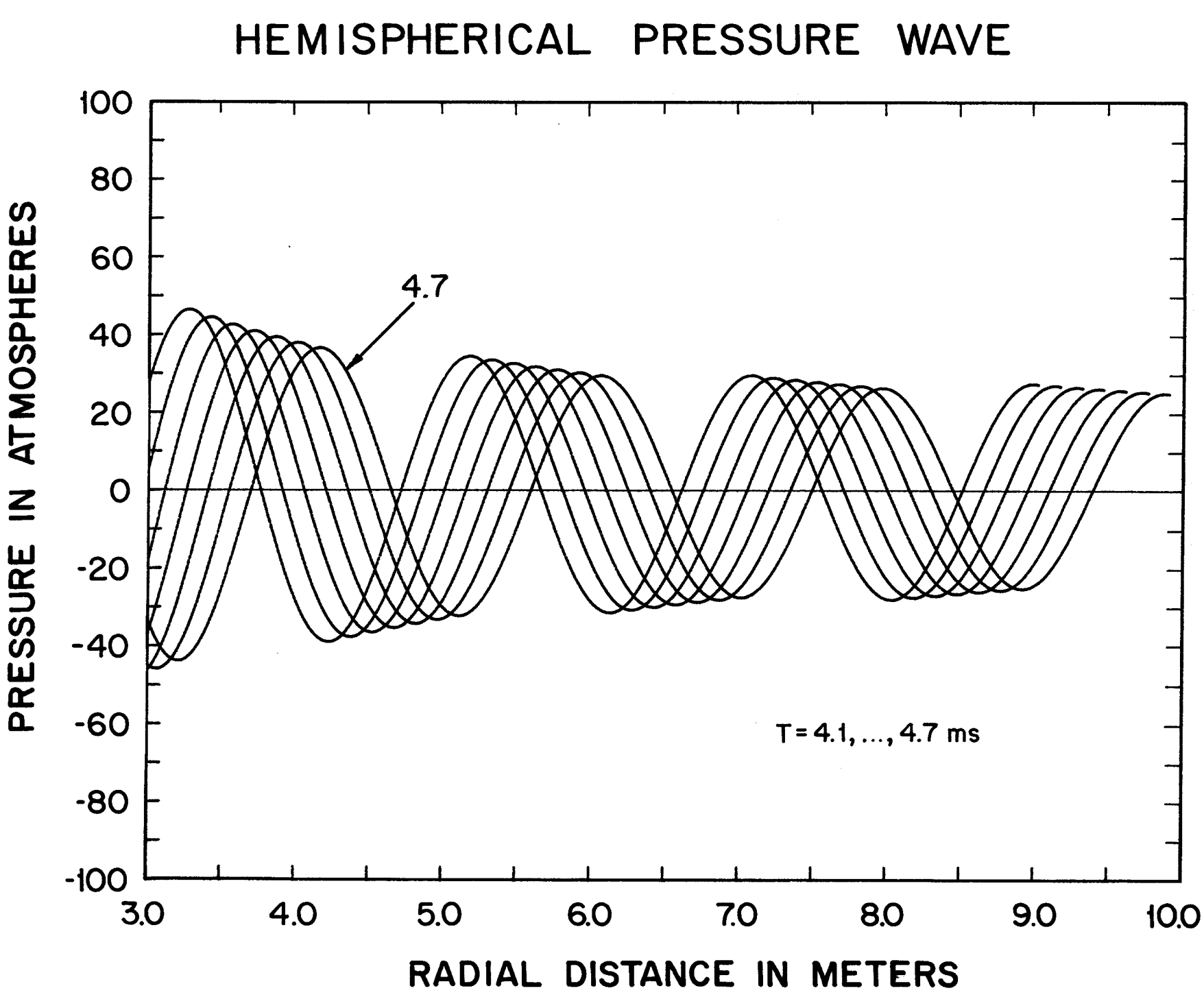
HEMISPHERICAL PRESSURE WAVE
PRESSURE IN ATMOSPHERES
100
80
60
40
20
0
-20
-40
-60
-80
-100
4.7
T = 4.1, ..., 4.7 ms
3.0
4.0
5.0
6.0
7.0
8.0
9.0
10.0
RADIAL DISTANCE IN METERS

Figure 6

this time is 2.4 MPa. Figure 7 shows the same wave at time 8.5 ms which is one damping time of the wall motion.

2.1.5 Pressure at the Wall

The fluid pressure at the water-wall interface is computed from the relation:

$$p(R_w,t) = \mathrm{Re}\left[\rho_c V_w \frac{i\omega - \gamma}{\frac{1}{R_w} + i\frac{\omega}{c}} e^{(i\omega-\gamma)t}\right] . \tag{30}$$

This yields:

$$p(R_w,t) = \frac{p_o R_w V_w}{1 + R_w^2 \frac{\omega^2}{c^2}} \left[\left(R_w \frac{\omega^2}{c} - \gamma\right)\cos \omega t - \left(\omega + \gamma R_w \frac{\omega}{c}\right)\sin \omega t\right] e^{-\gamma t} . \tag{31}$$

Figure 8 depicts this pressure for the data in Table 1.

2.1.6 Intensity and Total Energy Per Shot

Analysis of the external damping effect of the fluid upon the pulsating wall is currently underway.[9] Inclusion of coupling between the wall response and the surrounding fluid response will result in an estimate of the relative amounts of energy absorbed by the wall per shot which are (a) dissipated within the wall, (b) transmitted to the fluid and (c) reflected back to the target chamber interior.

The energy flow rate through a unit area at the vessel surface, averaged over a cycle, is:

$$I_w(t) = \frac{\omega}{2\pi} \int_{t-\frac{\pi}{2}}^{t+\frac{\pi}{\omega}} P(R_w,\tau) V_w d\tau . \tag{32}$$

Inserting $P(R_w,\tau)$ and $V_w(\tau)$, this yields:

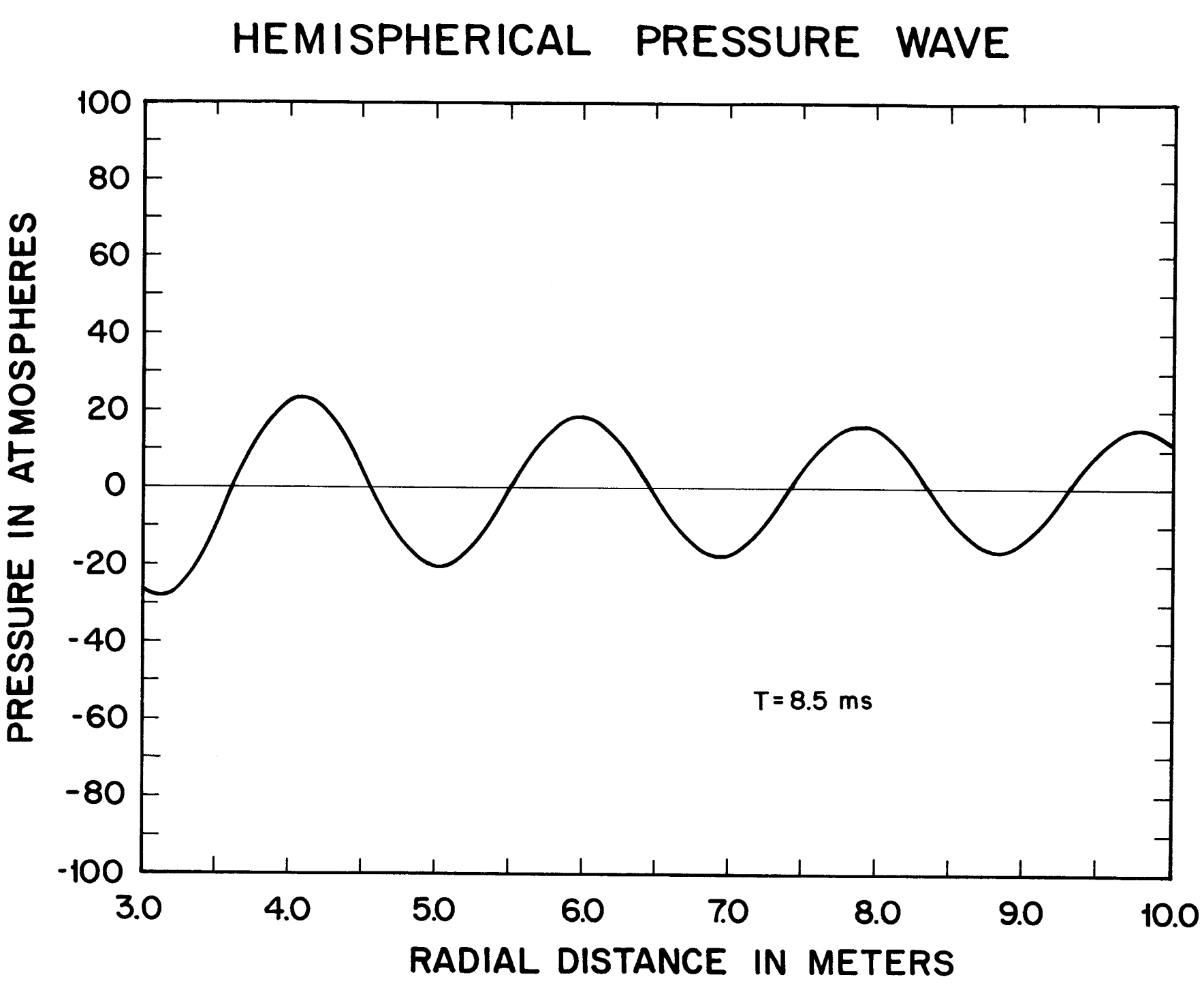
HEMISPHERICAL PRESSURE WAVE
PRESSURE IN ATMOSPHERES
100
80
60
40
20
0
-20
-40
-60
-80
-100
T = 8.5 ms
3.0
4.0
5.0
6.0
7.0
8.0
9.0
10.0
RADIAL DISTANCE IN METERS

Figure 7

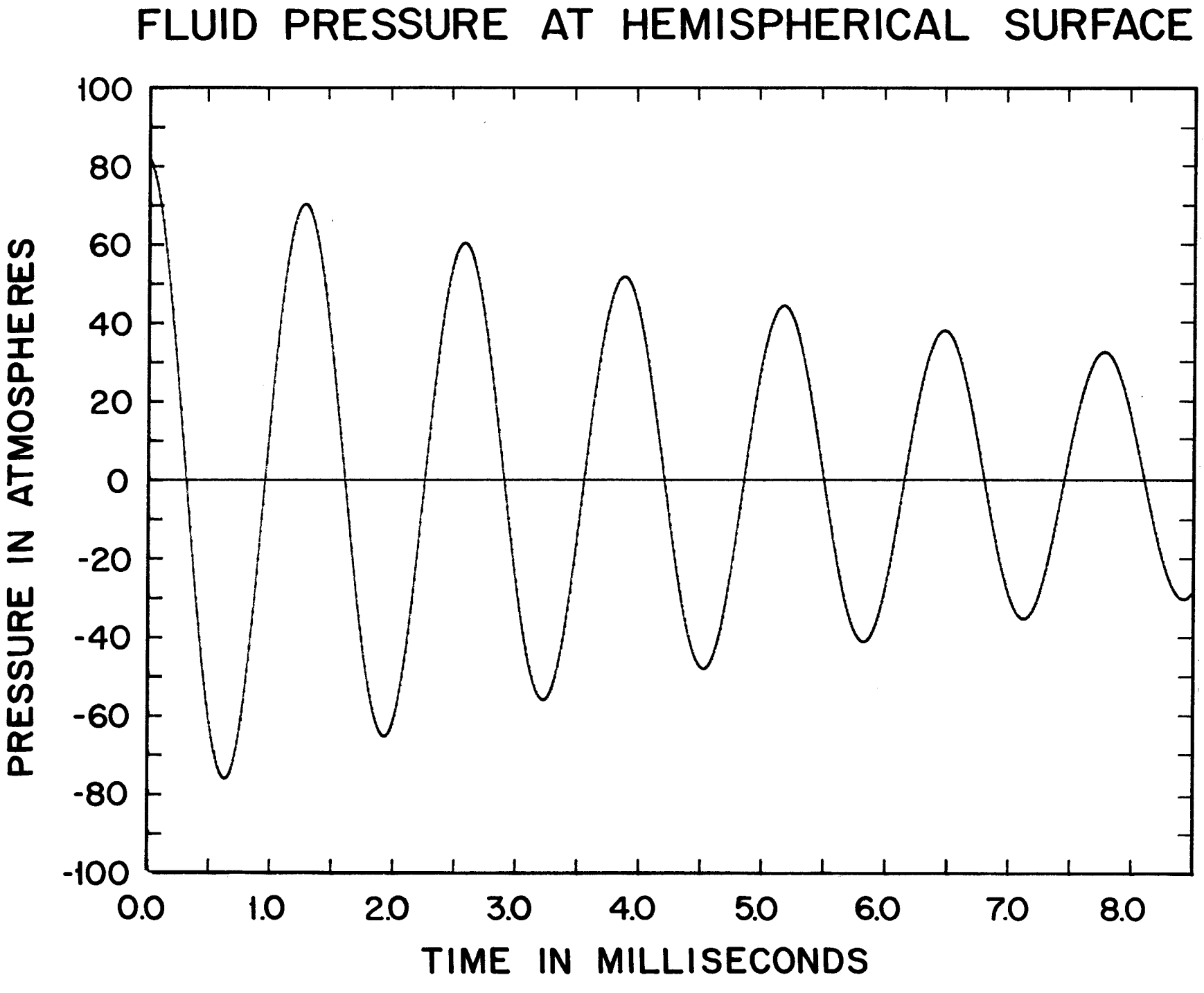
FLUID PRESSURE AT HEMISPHERICAL SURFACE
PRESSURE IN ATMOSPHERES
100
80
60
40
20
0
-20
-40
-60
-80
-100
0.0
1.0
2.0
3.0
4.0
5.0
6.0
7.0
8.0
TIME IN MILLISECONDS

Figure 8

$$I_w(t) = \frac{1}{2}\rho_o c V_w^2 \frac{R_w^2 \frac{\omega^2}{c^2} - \frac{\gamma}{c} R_w}{R_w^2 \frac{\omega^2}{c^2} + 1} e^{-2\gamma t} \quad . \tag{33}$$

Integrating over time and the hemispherical surface, the energy emitted per shot is:

$$E = \frac{\pi}{2\gamma} \frac{\rho_o R_w^3 V_w^2}{1 + R_w^2 \frac{\omega^2}{c^2}} \left(R_w \frac{\omega^2}{c} - \gamma\right) \quad . \tag{34}$$

Inserting values from Table 1 yields 5.65 MJ emitted per shot.

2.1.7 Cavitation

Recall that from our previous discussion the condition that no cavitation occur is $I_w < p_o^2/2\rho_o c$. Using I_w from 2.1.6 this condition becomes

$$V_w < \frac{p_o}{\rho_o c} \left[\frac{\frac{c}{R_w} + \frac{R_w^2 \omega^2}{c}}{R_w \frac{\omega^2}{c} - \gamma}\right]^{1/2} \tag{35}$$

which is inconsistent with the data from Table 1. This indicates that cavitation should be expected. The effects of this cavitation on the ultimate result of this analysis are not yet clear.

2.2 Cylindrical Wave Case

2.2.1 Cylindrical Waves

If we again neglect nonlinear terms for the cylindrical wave case the basic equations become

$$\frac{\partial^2\phi}{\partial r^2} + \frac{1}{r}\frac{\partial\phi}{\partial r} = \frac{1}{c^2}\frac{\partial^2\phi}{\partial t^2} \tag{36}$$

$$V(r,t) = \frac{\partial}{\partial r}\phi(r,t)$$

$$\rho_o \frac{\partial V}{\partial t} = -\frac{\partial x}{\partial r}$$

2.2.2 Undamped Case

An undamped harmonic wall pulsation generates a fluid velocity

$$V(r,t) = V_w \mathrm{Re}\left[\frac{H_1^{(2)}(\frac{r\omega}{c})}{H_1^{(2)}(R_w\frac{\omega}{c})} e^{i\omega t}\right] \tag{37}$$

where $H_1^{(2)}$ is the first order Hankel function of the second kind. This may be used to check the magnitude of the nonlinear terms as in the spherical case.

2.2.3 Damped Case

Taking the Laplace transform of the basic equations and applying the transformed boundary conditions results in

$$\bar{v}(r,s) = V_w \frac{s+\gamma}{(s+\gamma)^2+\omega^2} \frac{K_1(\frac{r}{c}s)}{K_1(\frac{R_w}{c}s)} \tag{38}$$

where K_1 is the modified Bessel function of order 1. This may be inverted using the residue method[10]

$$f(t) = \frac{1}{2\pi i}\int_{\sigma-i\infty}^{\sigma+i\infty} e^{zt}\bar{f}(z)dz + \frac{1}{2\pi i}\int_{C_\infty} e^{zt}\bar{f}(z)dz = \sum_{n=1}^{N} \mathrm{Res}[\bar{f}(z)e^{zt}]_{z=z_n} . \tag{39}$$

The function $K_v(z)$ is analytic in the z-plane cut along the negative real axis and has no zeroes in $|\arg z| < \pi/2$. The number of zeros in $\pi/2 \leq |\arg z| < \pi$

is the even integer nearest $\nu - 1/2$ unless $\nu - 1/2$ is an even integer in which case the number is $\nu - 1/2$.[11] K_1 thus has no zeroes, furthermore $K_1(z)/K_1(cz)$ is single-valued. Therefore $\bar{v}$ has poles only at $s = -\gamma \pm i\omega$. Choosing the contour shown below

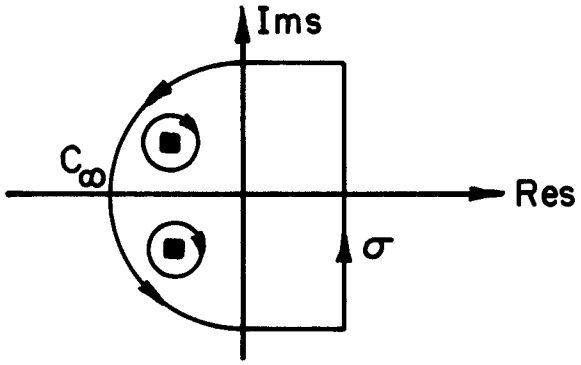

the inversion yields

$$v(r,t) = V_w \mathrm{Re}\left[\frac{K_1\left(\frac{r}{c}(-\gamma + i\omega)\right)}{K_1\left(\frac{R_w}{c}(-\gamma + i\omega)\right)} e^{-(\gamma - i\omega)t}\right] \tag{40}$$

which reduces correctly to the undamped case for $\gamma \to 0$. The modified Bessel function of a complex argument will be expanded as

$$K_1(z) = \sqrt{\frac{\pi}{2z}}\, e^{-z}\left[1 + \frac{3}{8z}\right] + O\left(\frac{1}{z^2}\right) . \tag{41}$$

From this the resulting fluid velocity is

$$V(r,t) = \frac{V_w\left(\frac{R_w}{r}\right)^{3/2}}{\left(R_w - \frac{3}{8}\frac{\gamma c}{\gamma^2 + \omega^2}\right)^2 + \left(\frac{3}{8}\frac{\omega c}{\gamma^2 + \omega^2}\right)^2} e^{-\gamma(t-(r-R_w/c))} \tag{42}$$

$$*\left[\left(rR_w - \frac{3}{8}\frac{\gamma c}{\gamma^2 + \omega^2}(r + R_w) + \left(\frac{3}{8}c\right)^2 \frac{1}{\gamma^2 + \omega^2}\right)\cos\omega\left(t - \frac{r - R_w}{c}\right)\right.$$

$$\left. - \frac{3}{8}\frac{\omega c}{\gamma^2 + \omega^2}(r - R_w)\sin\omega\left(t - \frac{r - R_w}{c}\right)\right] .$$

The fluid pressure is obtained from the expression

$$p(r,t) = V_w\rho_o \mathrm{Re}\left[e^{(i\omega-\gamma)t}\,\frac{K_o\left(\frac{r}{c}(-\gamma+i\omega)\right)}{K_1\left(\frac{R_w}{c}(-\gamma+i\omega)\right)}\right] . \tag{43}$$

The result, upon approximating K_o to the same order as K_1, is

$$p(r,t) = V_w\rho_o c\,\frac{\left(\frac{R_w}{r}\right)^{3/2}}{R_w^2 - \frac{3}{4}R_w\frac{c\gamma}{\gamma^2+\omega^2} + \left(\frac{3c}{8}\right)^2\frac{1}{\gamma^2+\omega^2}}\,e^{-\gamma\left(t-(r-R_w/c)\right)} \tag{44}$$

$$*\left[\left(rR_w + \frac{1}{8}\frac{c\gamma}{\gamma^2+\omega^2}(R_w - 3r) - 3\left(\frac{c}{8}\right)^2\frac{1}{\gamma^2+\omega^2}\right)\cos\,\omega\left(t - \frac{r-R_w}{c}\right)\right.$$

$$\left. - \frac{1}{8}\frac{c\omega}{\gamma^2+\omega^2}(r_w + 3r)\sin\,\omega\left(t - \frac{r-R_w}{c}\right)\right] .$$

This pressure is plotted in Figs. 9-11. These pressure waves are analogous to the spherical waves. Pressure amplitudes at the outer wall are greater for the cylindrical wave, as expected, since the geometry results in a weaker divergence.

2.2.4 Fluid Pressure at the Wall

The fluid pressure at the cylindrical wall is

$$P(R_w,t) = V_w\rho_o c\,\frac{1}{R_w^2(\gamma^2+\omega^2) - \frac{3}{4}R_w c\gamma + \left(\frac{3c}{8}\right)^2}\,e^{-\gamma t} * \left[\left(R_w^2(\gamma^2+\omega^2 - 2R_w c\gamma\right.\right. \tag{45}$$

$$\left.\left. - 3\left(\frac{c}{8}\right)^2\right)\cos\,\omega t - \frac{1}{2}R_w c\omega\,\sin\,\omega t\right]$$

and this is plotted in Fig. 12.

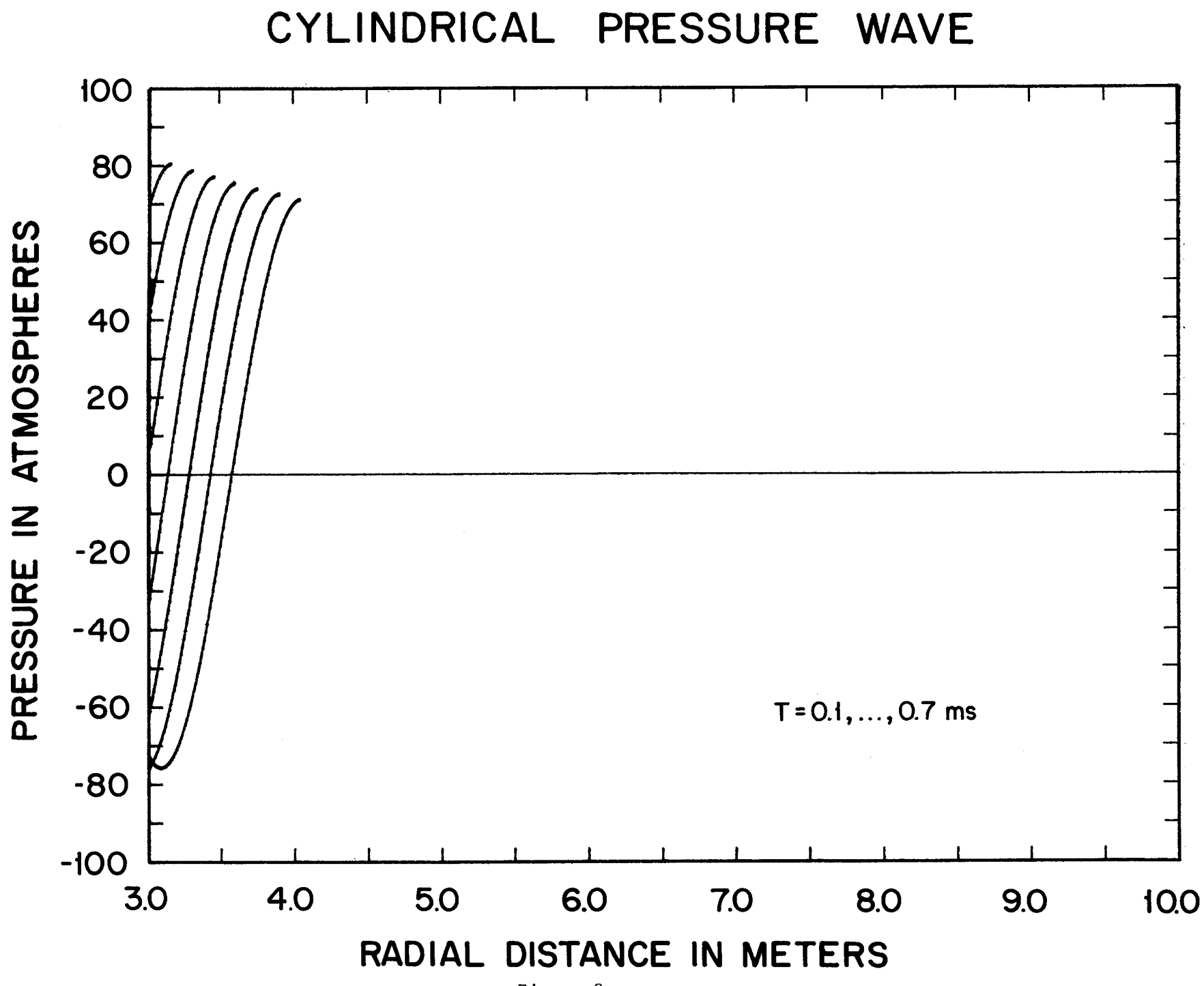
CYLINDRICAL PRESSURE WAVE
PRESSURE IN ATMOSPHERES
100
80
60
40
20
0
-20
-40
-60
-80
-100
3.0
4.0
5.0
6.0
7.0
8.0
9.0
10.0
RADIAL DISTANCE IN METERS
T=0.1,...,0.7 ms

Figure 9

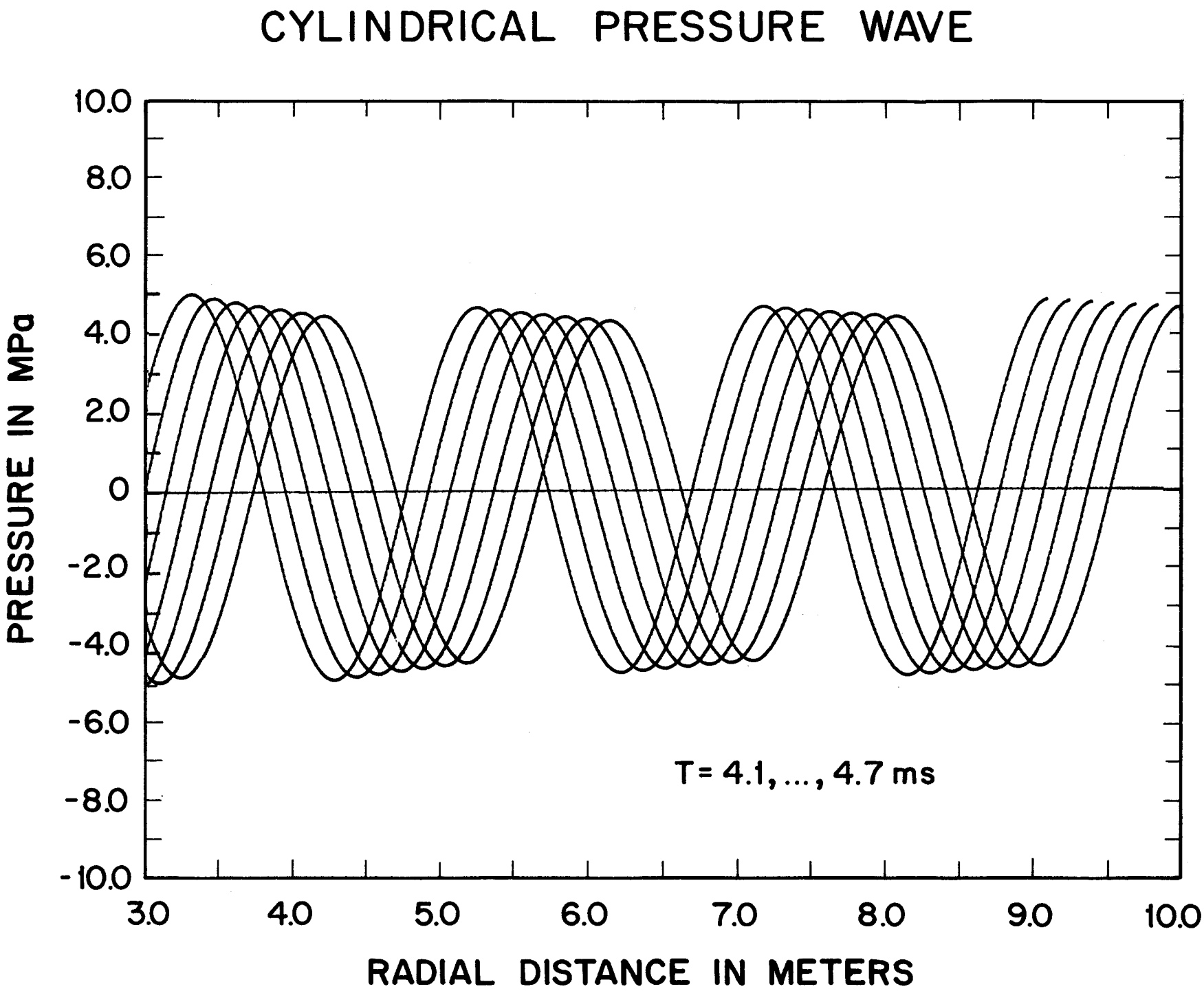
CYLINDRICAL PRESSURE WAVE
10.0
8.0
6.0
4.0
2.0
0
-2.0
-4.0
-6.0
-8.0
-10.0
PRESSURE IN MPa
T= 4.1, ..., 4.7 ms
3.0
4.0
5.0
6.0
7.0
8.0
9.0
10.0
RADIAL DISTANCE IN METERS

Figure 10

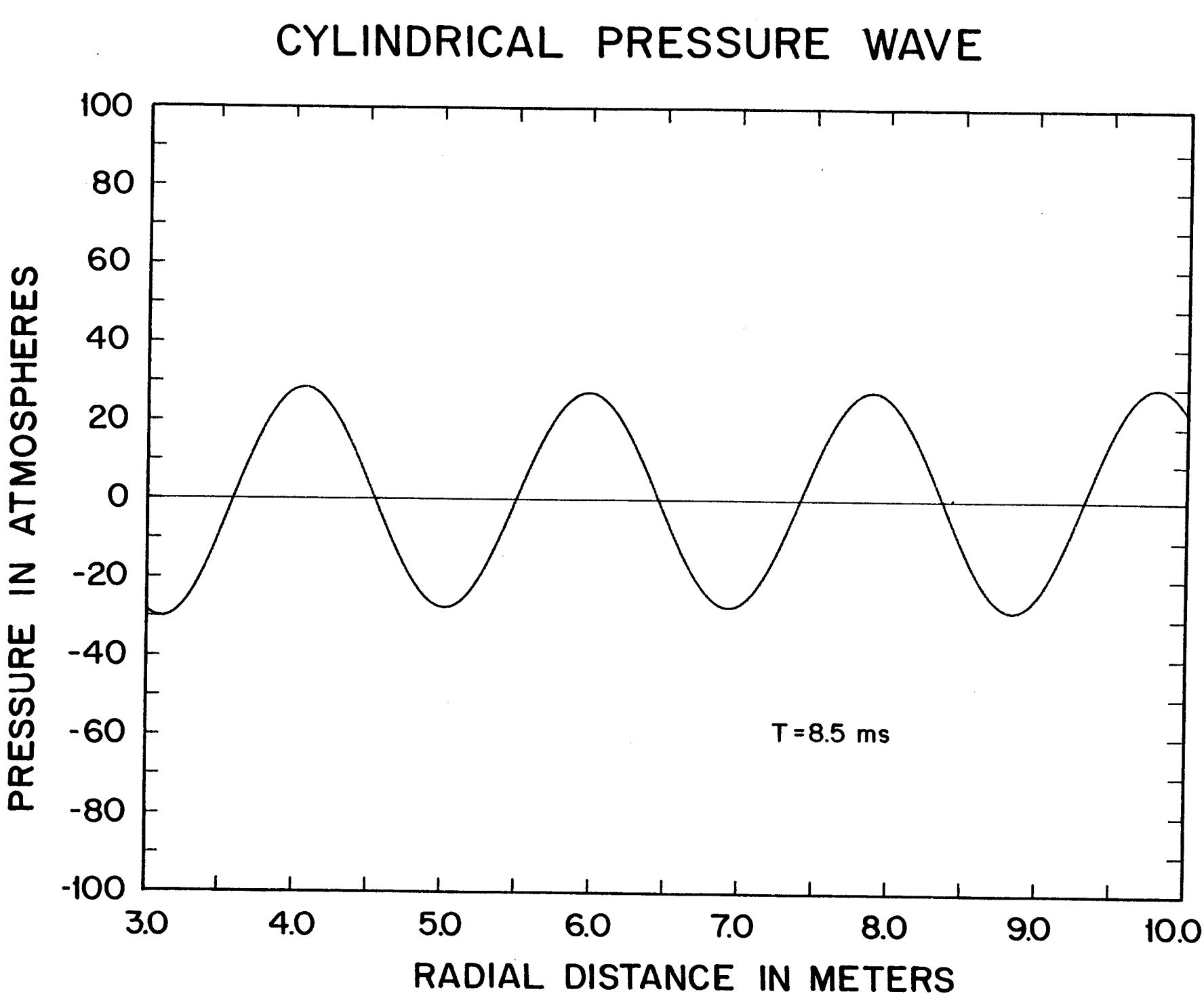
CYLINDRICAL PRESSURE WAVE
PRESSURE IN ATMOSPHERES
100
80
60
40
20
0
-20
-40
-60
-80
-100
T=8.5 ms
3.0
4.0
5.0
6.0
7.0
8.0
9.0
10.0
RADIAL DISTANCE IN METERS

Figure 11

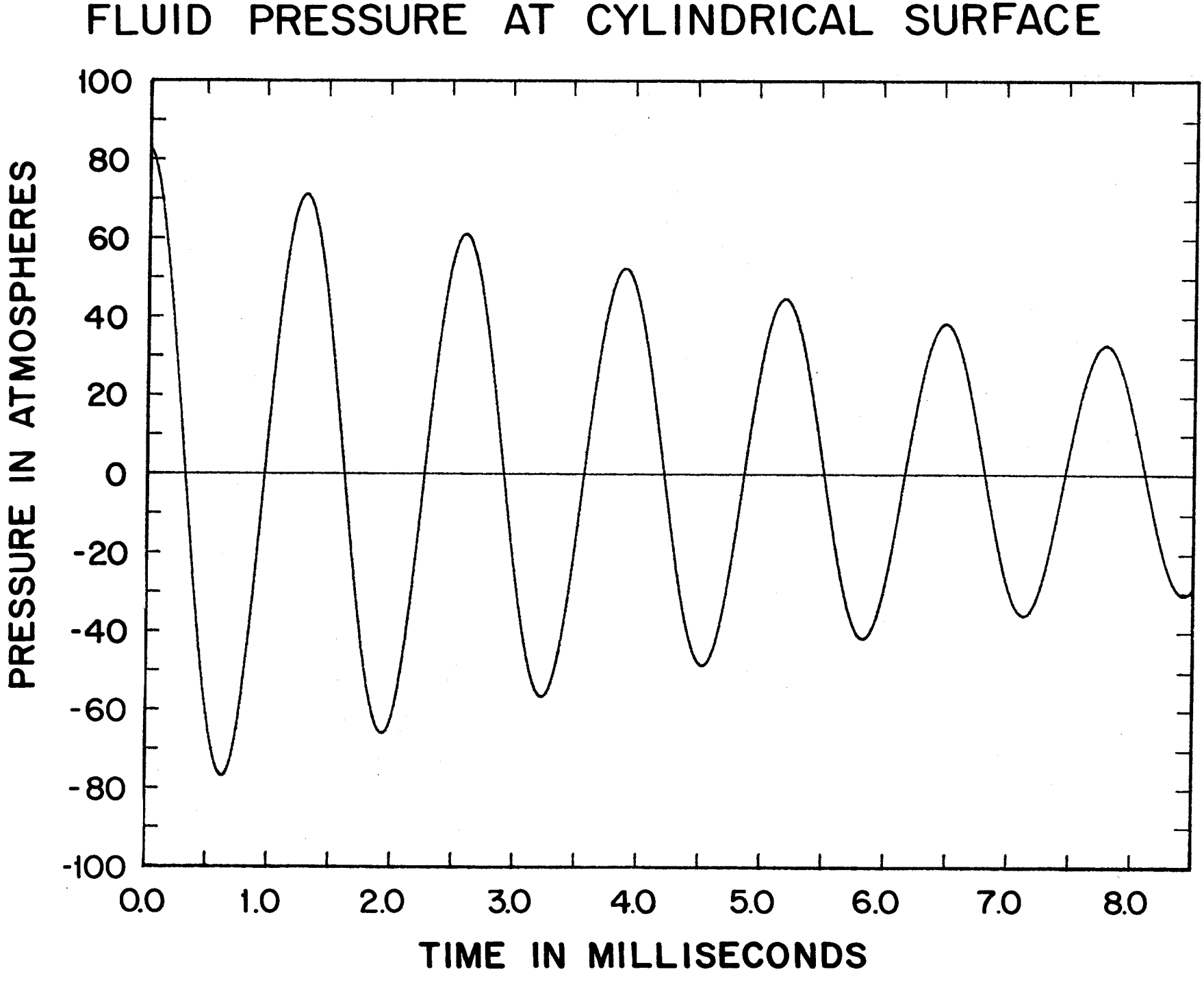
FLUID PRESSURE AT CYLINDRICAL SURFACE
PRESSURE IN ATMOSPHERES
100
80
60
40
20
0
-20
-40
-60
-80
-100
0.0
1.0
2.0
3.0
4.0
5.0
6.0
7.0
8.0
TIME IN MILLISECONDS

Figure 12

2.2.5 Intensity and Total Energy per Shot

The acoustic intensity of the damped cylindrical pulsation is

$$I_w(t) = \frac{1}{2} V_w^2 \rho_o c \left[\frac{R_w^2(\gamma^2 + \omega^2) - 2R_w c\gamma - 3(\frac{c}{8})^2}{R_w^2(\gamma^2 + \omega^2) - \frac{3}{4} R_w c\gamma + (\frac{3c}{8})^2}\right] e^{-2\gamma t} \tag{46}$$

where the factor in brackets is approximately unity for data in Table 1 since the wavelength, 1.9 m, is not large compared to the cylinder dimensions. The total acoustic energy emitted by the cylindrical wall per shot is

$$E = \frac{1}{2\gamma} V_w^2 \rho_o c R_w H_w \pi \frac{R_w^2(\gamma^2 + \omega^2) - 2R_w c\gamma - 3(\frac{c}{8})^2}{R_w^2(\gamma^2 + \omega^2) - \frac{3}{4} R_w c\gamma + (\frac{3c}{8})^2} . \tag{47}$$

For the data in Table 1 this yields an energy of 11.4 MJ per shot.

The sum of the energies emitted by the cylindrical and hemispherical walls, 22.7 MJ, is to be contrasted with the total hydrodynamic energy, 60 MJ, of the blast wave incident upon the target chamber inner wall. A more realistic model would perhaps include only the upper hemisphere for the purposes of energy emission since the bottom hemisphere is firmly anchored to supporting structural members as shown in Fig. 2.

2.2.6 Cavitation

Again if we look at cavitation at the water wall interface for the cylindrical case we find

$$V_w < \frac{p_o}{\rho_o c} \left[\frac{R_w^2(\gamma^2 + \omega^2) - \frac{3}{4} R_w c\gamma + 3(\frac{c}{8})^2}{R_w^2(\gamma^2 + \omega^2) - \frac{3}{4} R_w c\gamma + (\frac{3c}{8})^2}\right]^{1/2} \tag{48}$$

which is inconsistent with Table 1.

3. BUBBLE SCREENS

It is of interest to contemplate the use of a screen of small bubbles as a barrier to and absorber of pressure waves launched by a vessel submerged in a pool of water. This report represents a preliminary examination of such an application. Although many of the models employed are perhaps oversimplifications it is hoped that the major issues involved are clearly delineated. Further work could be carried out to improve the details of the analysis.

The pronounced effect of gas bubbles in a fluid upon the sound propagation within that fluid is well known. A few widely dispersed bubbles, so small as to be invisible, have an appreciable acoustic effect.[12] The propagation speed is greatly diminished and substantial attenuation occurs.[13] Fluids containing a large number of bubbles will be practically opaque to acoustic waves.[12]

For the purposes of this analysis a bubble screen is defined to be a random distribution of bubbles, of identical radius and physical properties, within a well defined slab region in a pool of water. Upward motion of the bubbles is neglected since the frequencies of interest are quite high. Variation of the bubble size and internal pressure with depth are ignored.

Given the void fraction x within the screen the nearest neighbor in the random distribution can be computed. The probability that the nearest neighbor lies between r and r + dr is

$$W(r)dr = 4\pi r^2 n \exp\left(-\frac{4}{3}\pi r^3 n\right) dr \qquad (49)$$

where n is the number density.[14] The expected separation distance is

$$D = \int_0^\infty rW(r)dr = 0.5539\ n^{-1/3} \qquad (50)$$

or, in terms of the bubble radius r_b and x

$$D = \frac{0.8929}{x^{1/3}}\ r_b\ .$$

For r_b in Table 1 and x = 0.001 this gives D = 1.8 cm. The corresponding number density is $n = 3 * 10^4\ m^{-3}$. Such a screen can be modeled as a homogeneous fluid, suppressing the discreteness of the bubbles. This is the approach employed in Section 3.2.1.

3.1 Bubble Screen Conditions

3.1.1 Damping Constants

"Bubbles excited to volume pulsations have a polytropic equation of state for the enclosed gas which results in a phase difference between the change in pressure per unit original pressure and the change in volume per unit original volume. Therefore, the work done in compressing the bubble is more than the work done by the bubble in expanding; this difference in the work done represents a net flow of energy into the liquid."[12] The damping associated with this mechanism is called thermal damping.

A second damping mechanism is called radiation damping. Pulsating bubbles act as sources of outgoing spherical sound waves. A fraction of the bubble energy is radiated in this fashion. Since this energy is initially in the incident or driving wave this represents a loss mechanism for the incident wave mode. The combined effect of many such oscillating bubbles is a randomization of the wave energy initially organized in the incident wave.

The third important damping effect is that of viscosity. Although as a bulk the fluid is considered to be inviscid, at the fluid-gas interface viscous forces are included. As the bubble rapidly expands and contracts this viscous effect results in heating of the fluid.

The possibility of bubble breakup and the associated energetics of the latent heat of surface formation will not be considered. The bubbles are small enough that breakup seems unlikely.

A total damping constant is defined to be the reciprocal of the Q-value of the bubble-fluid system. The Q-value characterizes the fraction of remaining energy lost per cycle. In terms of the three mechanisms discussed, the total damping is

$$\delta = \delta_{rad} + \delta_{th} + \delta_{vis} \cdot \tag{51}$$

The resonant frequency of a bubble-fluid system is given by Minnaert's expression

$$f_M = \sqrt{\frac{3\gamma P_o}{\rho}} \frac{1}{2\pi R_b} \tag{52}$$

where: γ = ratio of specific heats of bubble gas

P_o = static pressure at which bubble has radius R_b.

For Table 1 data the radius of a resonant bubble is 4 mm.

Analytic expressions for the damping constants are:[12]

$$\delta_{th} = 2 \frac{\left(\frac{16}{9} \frac{1}{(\gamma - 1)^2} \frac{Fg}{f} - 3\right)^{1/2} - \frac{3\gamma - 1}{3(\gamma - 1)}}{\frac{16}{9} \frac{1}{(\gamma - 1)^2} \frac{Fg}{f} - 4} \tag{53}$$

η = polytropic exponent

$F = 3\gamma P_o/4\pi\rho D_b$

D_b = thermal diffusivity of bubble gas.

Other variables are as previously defined. For f << 7kHz this expression reduces to $\delta_{th} = 4.4 * 10^{-4}\sqrt{f}$ accurate to 1%. The radiation damping constant is

$$\delta_{rad} = \frac{2\pi R_o f}{c} \left(\frac{g}{\alpha}\right)^{1/2} \tag{54}$$

where g/α is a factor which describes the departure of the bubble wall from adiabatic stiffness. For large bubbles $g/\alpha \approx 1$. Finally, the viscous damping constant is

$$\delta_{vis} = \frac{8\pi}{3} \frac{\mu}{\gamma} \frac{1}{P_o} f \tag{55}$$

μ = coefficient of viscosity at the gas-water interface.

Evaluating these at resonance yields the resonant damping constant. There are numerous sources of uncertainty in this matter, nevertheless, the total damping constant will be taken as $\delta = 0.02$. One can get data such as this from Table 1 as well as from the chart given in Ref. (12).

3.1.2 Attenuation Coefficient

A general theory of scattering from randomly distributed scatterers[15] is applied in Ref. (16) to derive the attenuation in decibels of a wave incident upon a bubble screen. For normal incidence the result is

$$K = 4.34 \frac{4\pi R \frac{R_o^3}{R^3} \delta_o \frac{\omega}{c}}{\left(\frac{R_o^2}{R^2} - 1\right)^2 + \frac{R_o^6}{R^6} \delta_o^2} ns \tag{56}$$

R = bubble radius

R_0 = resonant bubble radius

s = screen thickness

δ_0 = resonant damping constant.

From this, an exponential damping coefficient can be computed as

$$\alpha = 3 \frac{c}{\omega} \delta_0 x \frac{1}{R_0^2} \left[\frac{\xi^5}{(1 - \xi^2)^2 + \xi^6 \delta_0^2}\right] . \tag{57}$$

The function in brackets is sharply peaked about $\xi = 1$ and achieves the value δ_0^{-2} there. Inserting Table 1 data gives

$$\alpha(\xi,x) = 1139 \frac{\xi^6}{(1 - \xi^2)^2 + 0.0004\ \xi^6} x .$$

This function is plotted in Fig. 13.

3.2 Bubble Screen Analysis

3.2.1 Barrier Problem

We assume that acoustic waves are normally incident upon a homogeneous slab of bubbles dispersed within a fluid. The acoustic properties within the slab are characterized by a sound speed c_2 and attenuation coefficient α. Outside the screen the sound speed is c_1 and there is no attenuation.

A simple model will be used to estimate the sound speed within the screen. The important effect is the change in fluid compressibility. Consider two fluids differing only in compressibility

$$\kappa = - \frac{1}{v} \left(\frac{\partial v}{\partial p}\right) \tag{58}$$

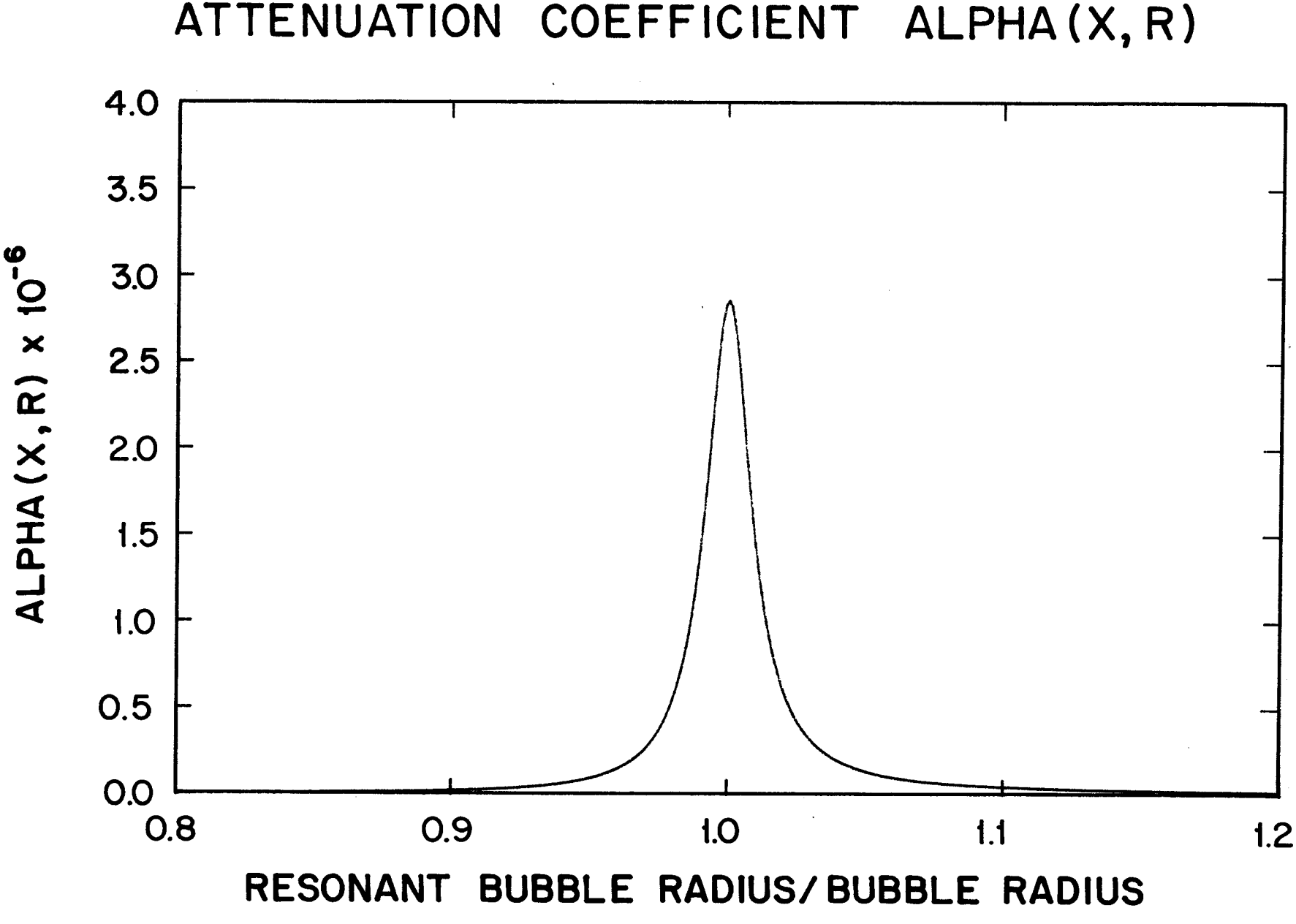
ATTENUATION COEFFICIENT ALPHA(X, R)
ALPHA(X, R) x 10^-6
4.0
3.5
3.0
2.5
2.0
1.5
1.0
0.5
0.0
0.8
0.9
1.0
1.1
1.2
RESONANT BUBBLE RADIUS/BUBBLE RADIUS

Figure 13

where v is the specific volume. Plane acoustic waves in each fluid are described by

$$\begin{aligned} \varepsilon &= \rho v^2 && \text{energy density} \\ p &= cpv && \text{pressure} \\ \rho &\approx \rho_0 && \text{density .} \end{aligned} \tag{59}$$

A steady state source drives waves into fluid 1 and fluid 2, then

$$\varepsilon_1 c_1 \Delta t = \varepsilon_2 c_2 \Delta t \tag{60}$$

through any test volume. This implies

$$\begin{aligned} \varepsilon_2 &= \varepsilon_1 \frac{c_1}{c_2} \\ V_2 &= V_1 \sqrt{\frac{c_1}{c_2}} \\ P_2 &= P_1 \sqrt{\frac{c_2}{c_1}} . \end{aligned} \tag{61}$$

For a liquid the sound speed is $c = \sqrt{B/\rho}$ where B is the bulk modulus. Taking fluid 1 to be water and fluid 2 to be water + bubbles gives

$$c_2 = c_1 \sqrt{\frac{B_2}{B_1}} . \tag{62}$$

When a sound wave passes through a substance the compressions and rarefactions are adiabatic. Then the appropriate compressibility is

$$\kappa_{adiabatic} = \frac{1}{\gamma} \kappa_{isothermal}$$

where γ is the ratio of specific heats. Actually, as mentioned, the bubble compressions and rarefactions are polytropic. For small bubbles the process occurs isothermally whereas for large bubbles the process is adiabatic for gas deep within the bubble and isothermal at the gas-water interface. Bubble compressibility will be taken as adiabatic to simplify matters. Assuming the air within the bubbles behaves as a perfect gas the adiabatic compressibility is

$$\kappa_b = \frac{1}{\gamma_b P_b} \tag{63}$$

where: $P_b = P_{atm} + \rho_o g h + \frac{2\sigma}{R_b}$

h = bubble depth

σ = latent heat of formation of unit surface area.

Using the relation $B_2/B_1 = \kappa_1/\kappa_2$ it follows that

$$c_2 = c_1 \left[\frac{1}{1 + x \frac{\kappa_b - \kappa_w}{\kappa_w}}\right]^{1/2} . \tag{64}$$

Assuming plane waves we can calculate the reflected and transmitted waves as shown in Fig. 1. We write

$$\begin{aligned} u_1 &= e^{i(\omega r - k_1 x)} + A_r e^{i(\omega t + k_1 x)} \\ u_2 &= [B_t e^{i(\omega t - k_2 x)} + B_1 e^{i(\omega t + k_2 x)}] e^{-\alpha x} \\ u_3 &= A_t e^{i(\omega t - (x-s)k_1)} \end{aligned} \tag{65}$$

and matching $\partial/\partial t$ and $-\rho c^2\ \partial/\partial x$ at the water-screen interface yields the transmission and reflection amplitudes:

$$|A_t| = 2\left[\frac{1 + \left(\frac{c_2^2}{c_1}\frac{\alpha}{\omega}\cos^2\frac{\omega}{c^2}s\right)^2}{\left((1+e^{-\alpha s})\cos\frac{\omega s}{c_2} - \frac{c_2\alpha}{\omega}\sin\frac{\omega s}{c_2}\right)^2 + \left(\frac{c_2^2\alpha}{c_1\omega}\cos\frac{\omega s}{c_2} + \left(\frac{c_2}{c_1} + \frac{c_1}{c_2}e^{-\alpha s}\right)\sin\frac{\omega s}{c_2}\right)^2}\right]^{1/2} e^{-\alpha s}$$

$$|A_r| = \left[\frac{\left((1 - e^{\alpha s})\cos\frac{\omega s}{c_2} - \frac{c_2\alpha}{\omega}\sin\frac{\omega s}{c_2}\right)^2 + \left(\frac{c_2^2\alpha}{c_1\omega}\cos\frac{\omega s}{c_2} - \left(\frac{c_2}{c_1} - \frac{c_1}{c_2}e^{\alpha s}\right)\sin\frac{\omega s}{c_2}\right)^2}{\left((1 + e^{\alpha s})\cos\frac{\omega s}{c_2} - \frac{c_2\alpha}{\omega}\sin\frac{\omega s}{c_2}\right)^2 + \left(\frac{c_2^2\alpha}{c_1\omega}\cos\frac{\omega s}{c_2} + \left(\frac{c_2}{c_1} + \frac{c_1}{c_2}e^{\alpha s}\right)\sin\frac{\omega s}{c_2}\right)^2}\right]^{1/2}. \quad (66)$$

Reflected pressure amplitudes are depicted in Figs. 14 and 15 for screen widths between 0.1 and 1.0 meters using a bubble radius of 2 mm, which is half the resonant radius. These plots show that appreciable reflection occurs. This situation seems undesirable since the reflected waves are focused back upon the pulsating vessel. However, an appropriate choice of screen thickness and void fraction gives a screen with a tolerable reflection ratio. This situation represents a "tuned screen" which effectively divides the waves into acceptable reflected and transmitted components.

Figures 16-18 depict the absorption, transmission, and reflection power ratios respectively. Figure 16 shows that a screen of width 0.4 m with void fraction x = 0.00075 results in a favorable rate of energy absorption, while Fig. 18 shows that with this choice the reflection is tolerable.

3.2.2 Multiple Screens

In order to alleviate the reflection problems associated with a bubble screen it may prove desirable to employ more than one screen. A plenum which

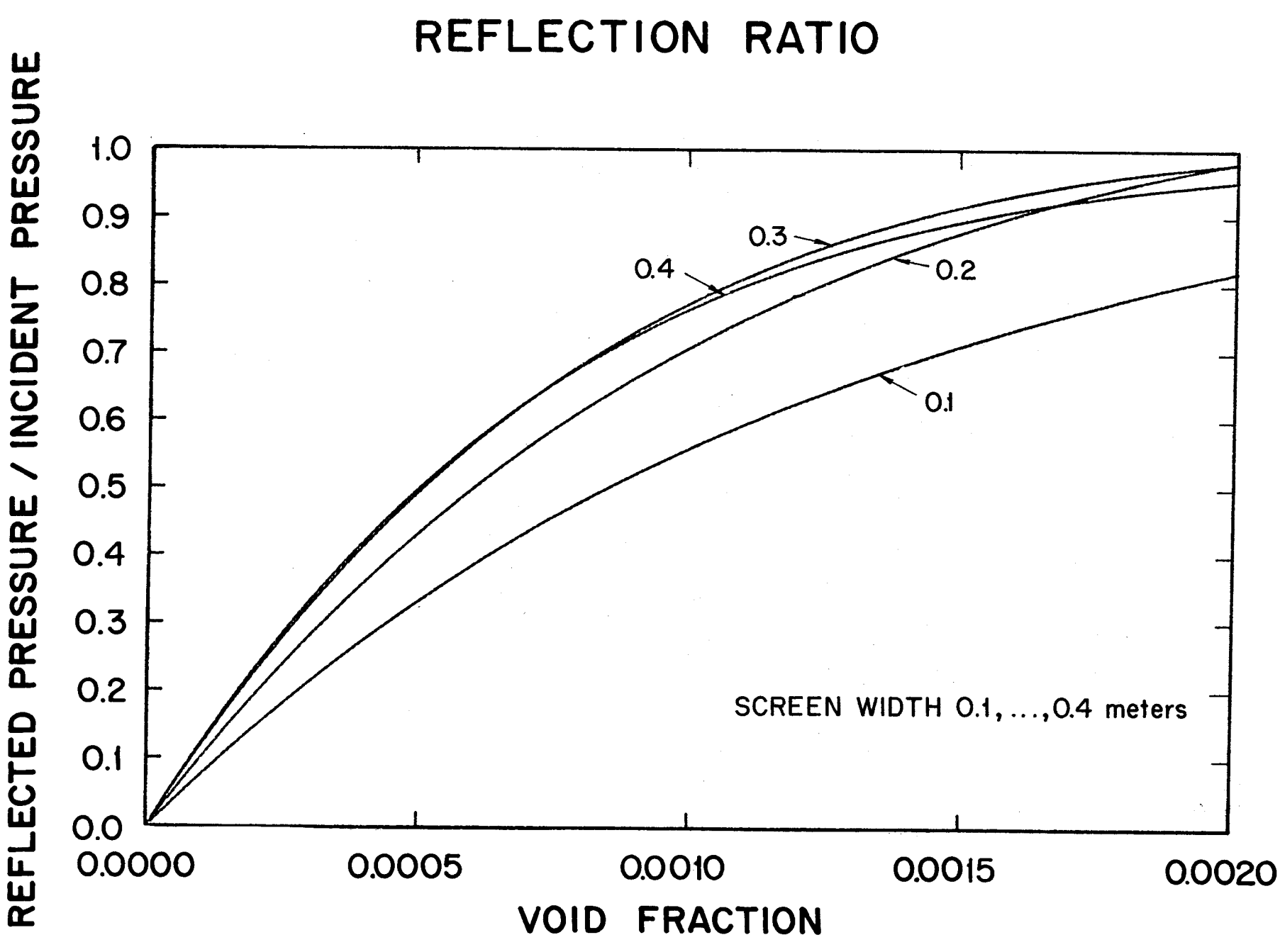
REFLECTION RATIO
REFLECTED PRESSURE / INCIDENT PRESSURE
1.0
0.9
0.8
0.7
0.6
0.5
0.4
0.3
0.2
0.1
0.0
0.0000
0.0005
0.0010
0.0015
0.0020
VOID FRACTION
0.3
0.4
0.2
0.1
SCREEN WIDTH 0.1, ...,0.4 meters

Figure 14

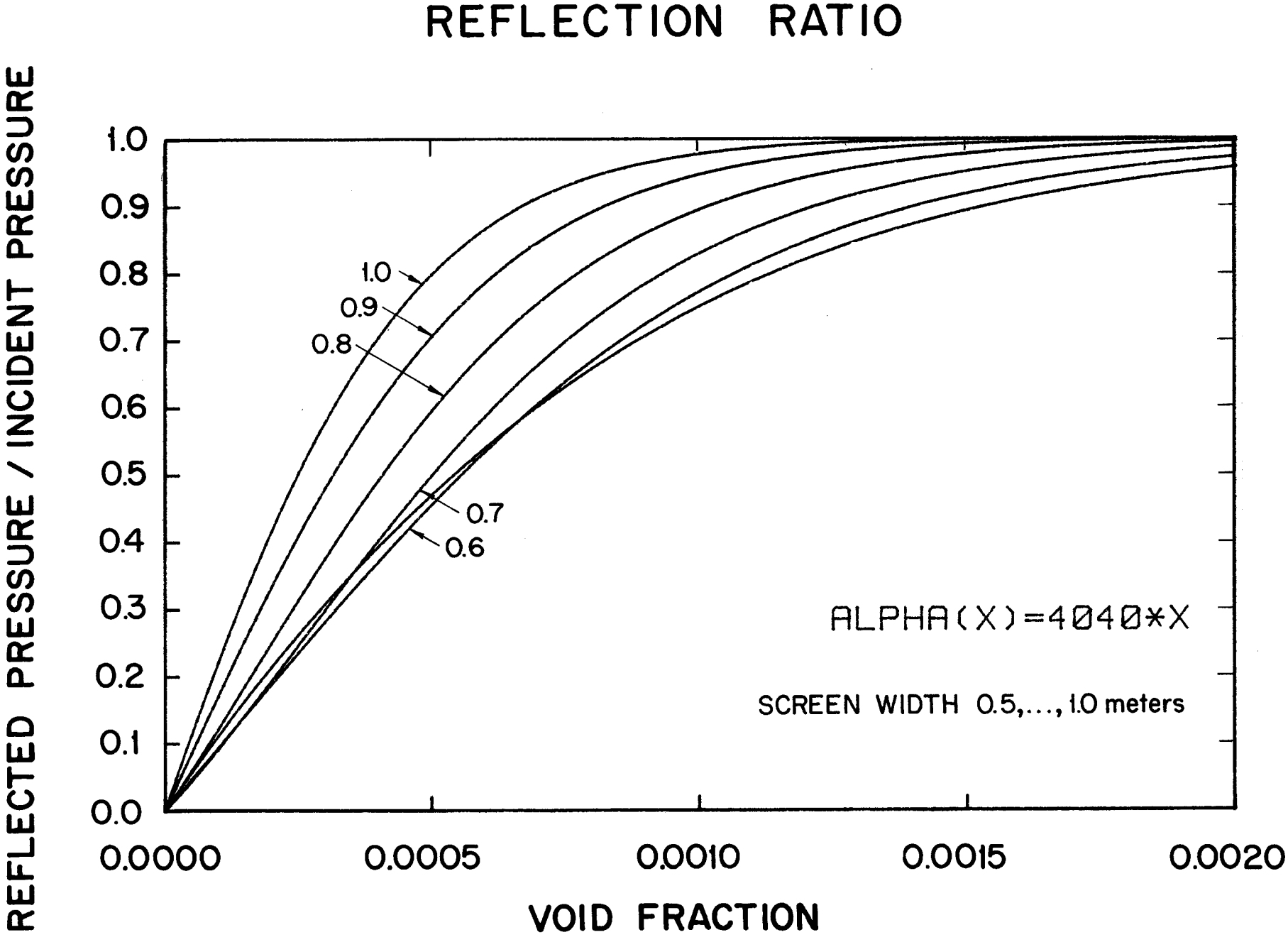
REFLECTION RATIO
REFLECTED PRESSURE / INCIDENT PRESSURE
1.0
0.9
0.8
0.7
0.6
0.5
0.4
0.3
0.2
0.1
0.0
0.0000
0.0005
0.0010
0.0015
0.0020
VOID FRACTION
1.0
0.9
0.8
0.7
0.6
ALPHA(X)=4040*X
SCREEN WIDTH 0.5,..., 1.0 meters

Figure 15

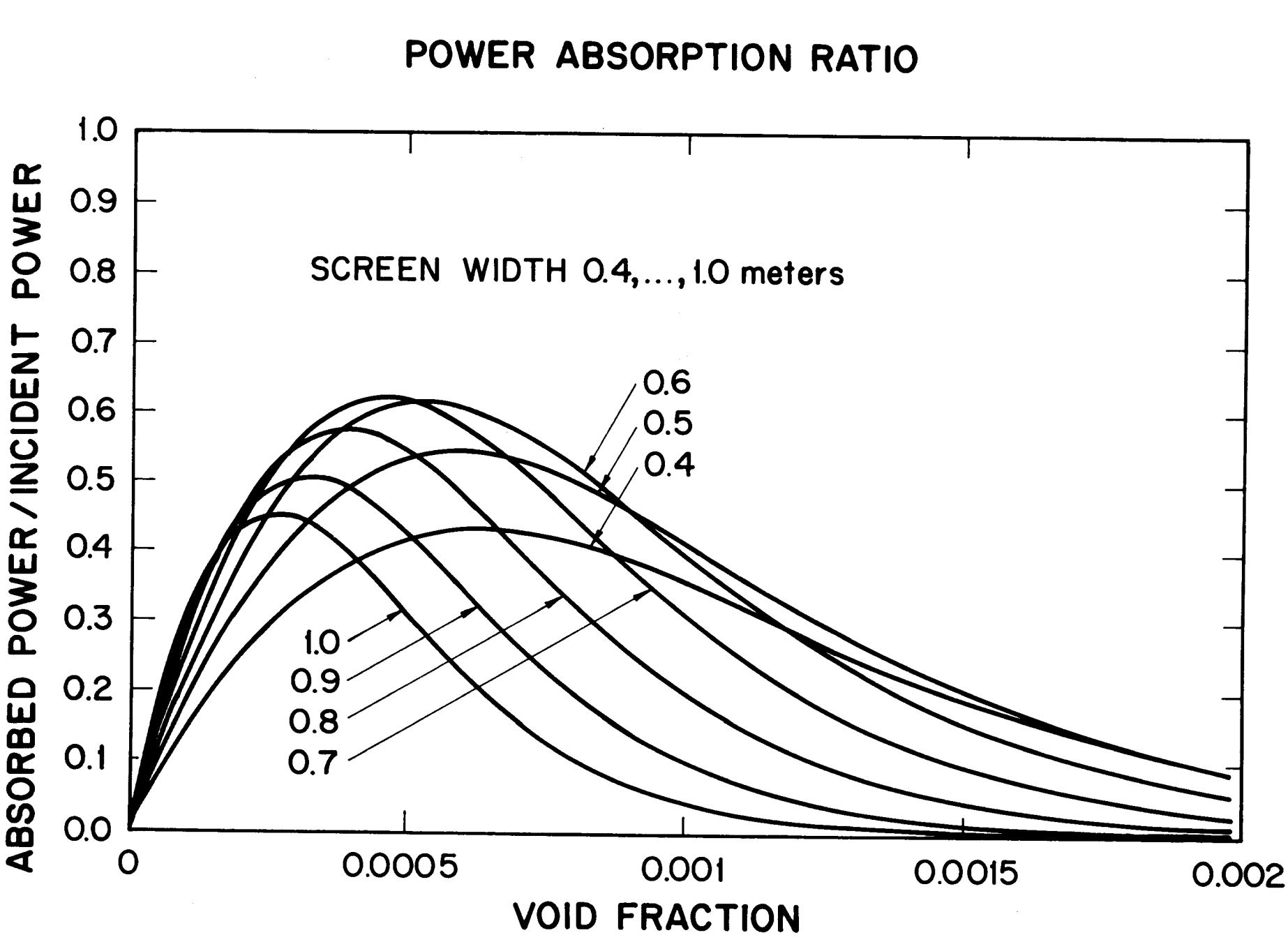
POWER ABSORPTION RATIO
SCREEN WIDTH 0.4,..., 1.0 meters
ABSORBED POWER / INCIDENT POWER
VOID FRACTION
1.0
0.9
0.8
0.7
0.6
0.5
0.4
0.3
0.2
0.1
0.0
0
0.0005
0.001
0.0015
0.002
0.6
0.5
0.4
1.0
0.9
0.8
0.7

Figure 16

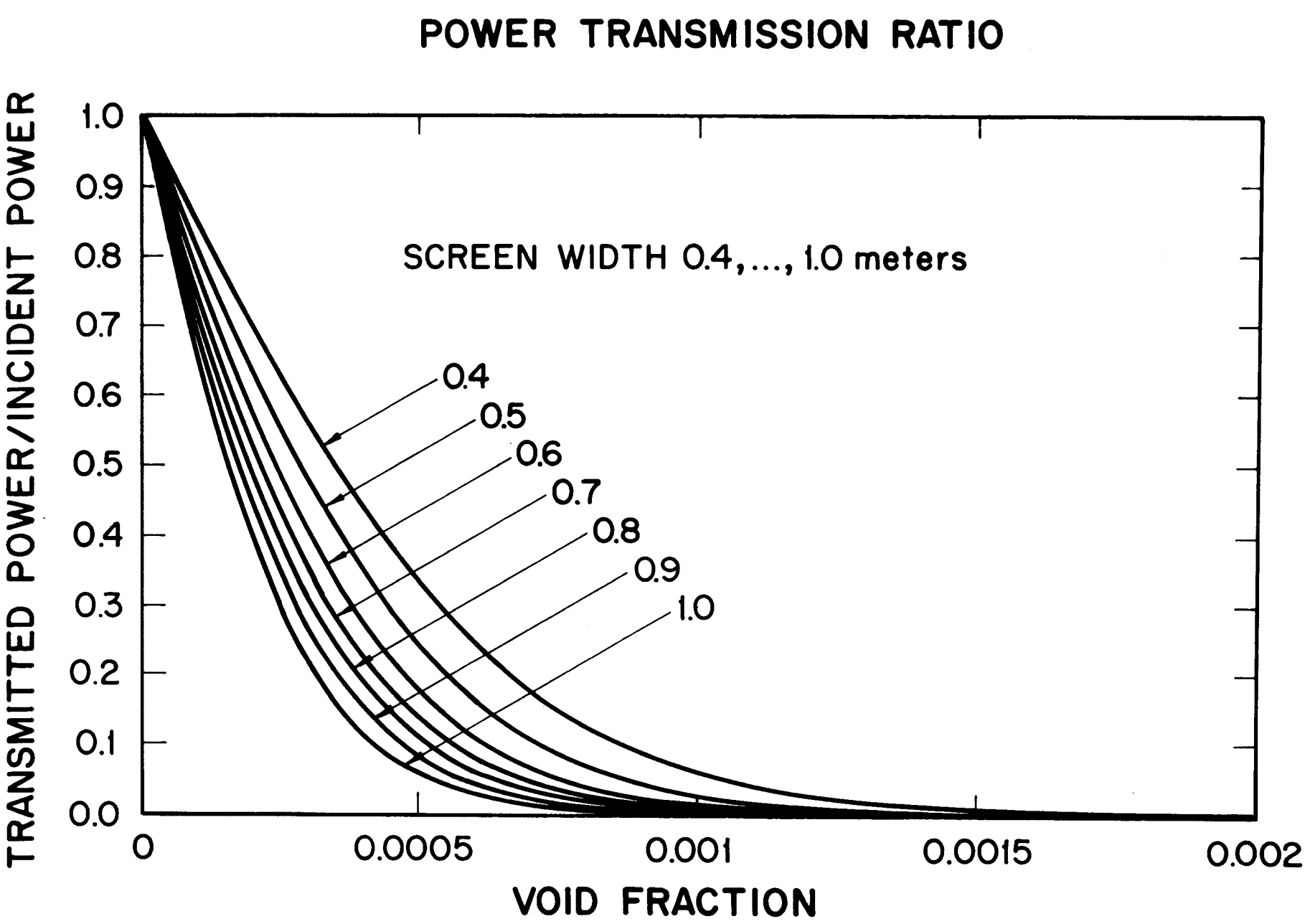
POWER TRANSMISSION RATIO
TRANSMITTED POWER/INCIDENT POWER
1.0
0.9
0.8
0.7
0.6
0.5
0.4
0.3
0.2
0.1
0.0
SCREEN WIDTH 0.4,..., 1.0 meters
0.4
0.5
0.6
0.7
0.8
0.9
1.0
0
0.0005
0.001
0.0015
0.002
VOID FRACTION

Figure 17

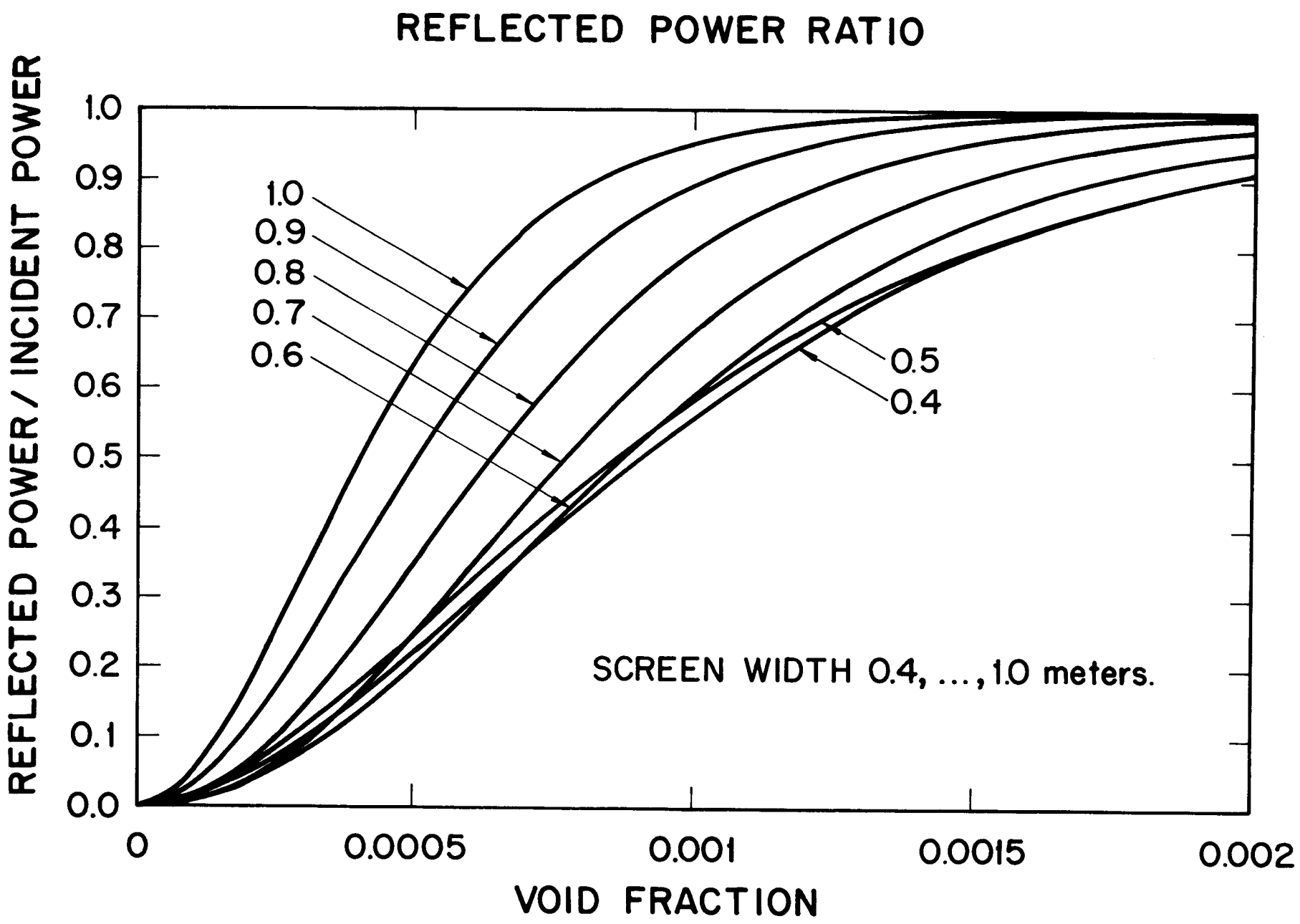
REFLECTED POWER RATIO
REFLECTED POWER / INCIDENT POWER
1.0
0.9
0.8
0.7
0.6
0.5
0.4
0.3
0.2
0.1
0.0
1.0
0.9
0.8
0.7
0.6
0.5
0.4
SCREEN WIDTH 0.4, ..., 1.0 meters.
0
0.0005
0.001
0.0015
0.002
VOID FRACTION

Figure 18

generates a bubble screen with a void fraction gradient could be used to create a void fraction ramp. The incident wave would not see a square barrier but would gradually find itself in regions of higher void fraction. This should result in enhanced transmission and reduced reflection. At some distance beyond this ramped screen a second, square barrier, could be employed. This arrangement would have the effect of trapping the wave. If a small void fraction were placed between the two screens wave energy could be absorbed effectively. Analysis of this multiple screen situation is currently underway.

A second possibility is to launch the waves directly into a screen contiguous with the target chamber surface. This would probably result in emission of shocks, complicating the analysis considerably.

Acknowledgment

This work was supported by Sandia National Laboratory under contract number DE-AS08-81DP40161.

References

1. B. Badger et al., "Report to Sandia Laboratory on University of Wisconsin Fusion Engineering Program Design Activities for the Light Ion Beam Fusion Target Development Facility from August 1981 to February 1982," University of Wisconsin Fusion Engineering Program Report UWFDM-457 (Feb. 1982).

2. E.G. Lovell, R.R. Peterson, R.L. Engelstad, G.A. Moses, "Transient Elastic Stresses in ICF Reactor First Wall Structural Systems," J. Nucl. Matl. 103&104 (1981) 115-120.

3. E.G. Lovell, R.R. Peterson, R.L. Engelstad, and G.A. Moses, "Transient Elastic Stresses in ICF Reactor First Wall Structural Systems," University of Wisconsin Fusion Engineering Program Report UWFDM-422 (Aug. 1981).

4. R.L. Engelstad and E.G. Lovell, "First Wall Mechanical Design for Light Ion Beam Fusion Reactors," University of Wisconsin Fusion Engineering Program Report UWFDM-322 (Dec. 1979).

5. E.G. Lovell, private conversation.

6. L.D. Landau, E.M. Lifshitz, Fluid Mechanics, Addison-Wesley Publishing Company Inc. (1958).

7. D. Sette and F. Wanderlingh, "Nucleation by Cosmic Rays in Ultrasonic Cavitation," Phys. Rev. 125 (1962) 409-417.

8. J.G. Kirkwood, H. Bethe, E. Montroll, "The Pressure Wave Produced by an Underwater Explosion; I, II," NDRC Division B, Report No. 252 (OSRD-588) and Report No. 281 (OSRD-676) (1942).

9. E.G. Lovell, R.L. Engelstad, private communication.

10. R.V. Churchill, Operational Mathematics, McGraw-Hill Book Company, Inc., (1958).

11. M.A. Abramowitz, I.A. Stegun, "Handbook of Mathematical Functions," National Bureau of Standards Applied Mathematics Series 55 (1964).

12. C. Devin, "Survey of Thermal, Radiation and Viscous Damping of Pulsating Air Bubbles in Water," J. Acoust. Soc. Am. 31, (1959) 1654-1667.

13. D.S. Drumheller, "A Theory of Bubbly Liquids," J. Acoust. Soc. Am. 66 (1979) 197-208.

14. S. Chandrasekhar, "Stochastic Problems in Physics and Astronomy," Rev. Mod. Phys. 15 (1943) 1-89.

15. L.L. Foldy, "The Multiple Scattering of Waves," Phys. Rev. 67 (1945) 107-119.

16. E.L. Carstensen, L.L. Foldy, "Propagation of Sound Through a Liquid Containing Bubbles," J. Acoust. Soc. Am. 19 (1947) 481-501.

17. F.B. Hildebrand, Advanced Calculus for Applications, Prentice-Hall (1976).